ARL-TR-9551 ● SEP 2022

DEVCOM ARMY RESEARCH LABORATORY

Results of Continuous Wave (CW) Laser Damage Measurements on Commercially Available Chalcogenide Optics at 1.07 µm

by John E McElhenny and Neal K Bambha

NOTICES

Disclaimers

The findings in this report are not to be construed as an official Department of the Army position unless so designated by other authorized documents.

Citation of manufacturer's or trade names does not constitute an official endorsement or approval of the use thereof.

Destroy this report when it is no longer needed. Do not return it to the originator.

ARL-TR-9551 ● SEP 2022

Results of Continuous Wave (CW) Laser Damage Measurements on Commercially Available Chalcogenide Optics at 1.07 µm

John E McElhenny and Neal K Bambha
DEVCOM Army Research Laboratory

REPORT DOCUMENTATION PAGE

Form Approved
OMB No. 0704-0188

1. REPORT DATE *(DD-MM-YYYY)*	2. REPORT TYPE	3. DATES COVERED (From - To)
September 2022	Technical Report	18 May 2018–18 August 2022

4. TITLE AND SUBTITLE
Results of Continuous Wave (CW) Laser Damage Measurements on Commercially Available Chalcogenide Optics at 1.07 µm

5a. CONTRACT NUMBER

5b. GRANT NUMBER

5c. PROGRAM ELEMENT NUMBER

6. AUTHOR(S)
John E McElhenny and Neal K Bambha

5d. PROJECT NUMBER

5e. TASK NUMBER

5f. WORK UNIT NUMBER

7. PERFORMING ORGANIZATION NAME(S) AND ADDRESS(ES)
DEVCOM Army Research Laboratory
ATTN: FCDD-RLS-CL
Adelphi, MD 20783

8. PERFORMING ORGANIZATION REPORT NUMBER
ARL-TR-9551

9. SPONSORING/MONITORING AGENCY NAME(S) AND ADDRESS(ES)

10. SPONSOR/MONITOR'S ACRONYM(S)

11. SPONSOR/MONITOR'S REPORT NUMBER(S)

12. DISTRIBUTION/AVAILABILITY STATEMENT
Approved for public release: distribution unlimited.

13. SUPPLEMENTARY NOTES
ORCID ID: John E McElhenny, 0000-0002-7029-2999

14. ABSTRACT
The continuous wave laser-induced damage threshold of various chalcogenide glasses, made by SCHOTT and Amorphous Materials Inc, are measured for a 5-s irradiance time of 1.07-µm light focused to a spot size with $1/e^2$ diameter of 830 or 1044 µm, following standards from the International Organization for Standardization.

15. SUBJECT TERMS
glass; amorphous materials; optics; infrared; damage; continuous wave; high power; chalcogenide; laser-induced damage threshold; SCHOTT; Amorphous Materials Inc; IRG; AMTIR; Electromagnetic Spectrum Sciences; Energy Sciences; Photonics, Electronics, and Quantum Sciences; Sciences of Extreme Materials; Weapons Sciences

16. SECURITY CLASSIFICATION OF:			17. LIMITATION OF ABSTRACT	18. NUMBER OF PAGES	19a. NAME OF RESPONSIBLE PERSON
a. REPORT	b. ABSTRACT	c. THIS PAGE			John E McElhenny
Unclassified	Unclassified	Unclassified	UU	70	19b. TELEPHONE NUMBER (Include area code) (301) 394-0214

Standard Form 298 (Rev. 8/98)
Prescribed by ANSI Std. Z39.18

Contents

List of Figures

List of Tables

1. Introduction

The US Army Combat Capabilities Development Command (DEVCOM) Army Research Laboratory, Sensors and Electron Devices Directorate's High Power Continuous Wave (HiPo CoW) Laser Laboratory for Optics and Sensors performed continuous wave (CW) laser-induced damage threshold (LIDT) measurements of commercially available chalcogenide optical windows from SCHOTT (IRG-24, IRG-25, IRG-26, and IRG-27) and Amorphous Materials Inc (AMTIR-1, AMTIR-2, AMTIR-4, AMTIR-5, AMTIR-6, and AMTIR-7). Measurements were performed in support of DEVCOM's Command, Control, Computers, Communications, Cyber, Intelligence, Surveillance, and Reconnaissance (C5ISR), Night Vision and Electronic Sensors Directorate (NVESD).

This report describes the materials, rough calculations, simulations, measurement setup, and methodologies used and presents the CW LIDT test results. During October 2018 through April 2021, the system was designed, built, tested, and characterized, and various chalcogenide optical windows were tested.

This report compliments Norm Comer's (2016) report, which detailed a similar study using longer CW mid- and long-wave infrared (IR) wavelengths. Here, all measurements are made using 1.07 μm wavelength CW light irradiating the samples for 5 s; some data was previously reported by McElhenny and Bambha (2018, 2019a, 2019b, 2020).

To view the CW LIDT data without experimental and background details, skip to Section 6, Summary and Conclusions.

2. Material Description

Chalcogenide glasses (ChGs) are amorphous materials that contain one or more chalcogen element from group 6a (excluding oxygen): sulfur (S), selenium (Se), and tellurium (Te) covalently bonded to network formers, such as arsenic (As), germanium (Ge), gallium (Ga), silicon (Si), or phosphorus (P). Chalcogens transmit at wavelengths of up to around 11 μm (S), 15 μm (Se), and 20 μm (Te). These glasses (amorphous solids) are structurally characterized by the total absence of long-range atomic order and are best described as a continuous random network. This manifests itself in standard binary chalcogenides, such as arsenic triselenide (As_2Se_3), which we will look at, as the As–Se network is locally 2-D with weak van der Waal bonding between layers, while the addition of fourfold-coordinated atoms, such as Ge (in the case of GeAsSe) makes the network 3-D by creating

bonds between layers. This results in a structure with increased rigidity, hardness, and strength (Fecht 1995; Eggleton et al. 2011).

This report examines 10 different commercially available ChGs, which can be broken down into four main compositions: GeSbSe, GeAsSe, AsSe, and AsS. The preparation of Se glasses is easier than S glasses due to the higher rate of chemical reactions between Se and other elements, as well as the lower pressure at which Se melts. Ternary ChGs, like those composed of GeSbSe and GeAsSe, are intrinsically optically stable, have a wide temperature range for the glass-forming process, and great transmission in the IR from 0.8 to 15 μm. They are described as the "most suitable" glass for IR optical systems. Examples of these are IRG-25 ($Ge_{28}Sb_{12}Se_{60}$), AMTIR-1 ($Ge_{33}As_{12}Se_{55}$), and IRG-24 ($Ge_{10}As_{40}Se_{50}$). Arsenic trisulfide (As_2S_3) (i.e., IRG-27 and AMTIR-6), has transmittance from the visible through IR (620 nm to 11 μm), a high-refractive index, low speed of sound, and high-quality factors. On the other hand, it also has high intrinsic loss and poor chemical stability. These optics have a reddish tint. Chalcogenide glasses benefit IR optical systems over single crystals, such as Ge and ZnSe, in that their refractive index has a lower temperature dependence (Zhou 2018).

Table 1 lists some of the properties of the 10 commercially available optics: IRG-24, IRG-25, IRG-26, IRG-27, AMTIR-1, AMTIR-2, AMTIR-4, AMTIR-5, AMTIR-6, and AMTIR-7.

Table 1 Properties of the 10 commercially available chalcogenides studied in this report

Material	Comp	t (mm)	Trans. Temp (Tg) (°C)	ΔT (T_g- 23 °C or K)	Mat. Dens., (ρ) (g/cm^3)	Cond., (κ) $Wcm^{-1}K^{-1}$	Spec. Heat (C_p) $Jg^{-1}K^{-1}$	Diffus. (D) cm^2sec^{-1}	Index	Abs. Coef., (α) (cm^{-1})
									1.06 μm	1 μm
AMTIR-1	$Ge_{33}As_{12}Se_{55}$	2	353	330	4.43	0.0025	0.301	0.00188	2.598	0.013
AMTIR-2	$As_{40}Se_{60}$	2	167	144	4.66	0.0024	0.285	0.00183	2.903	0.040
AMTIR-4	AsSe	2	103	80	4.49	0.0022	0.360	0.00137	2.754	0.015
AMTIR-5	AsSe	2	147	124	4.51	0.0024	0.318	0.00166	2.870	0.030
AMTIR-6	As_2S_3	2	180	157	3.20	0.0017	0.456	0.00115	2.472	0.009
AMTIR-7	AsSe	2	119	96	4.50	0.0023	0.339	0.00148	2.809	0.040
IRG-24	$Ge_{10}As_{40}Se_{50}$	3	225	202	4.47	0.0018	0.370	0.00109	2.711	0.044
IRG-25	$Ge_{28}Sb_{12}Se_{60}$	3	285	262	4.66	0.0025	0.330	0.00163	2.715	0.203
IRG-26	$As_{40}Se_{60}$	3	185	162	4.63	0.0024	0.360	0.00144	2.913	0.122
IRG-27	As_2S_3	3	197	174	3.20	0.0033	0.482	0.00214	2.476	0.028

The glass-transition temperature, T_g, is the temperature at which we presume damage will occur when the ChGs reaches it. The thermal conductivity is a measure of its ability to conduct heat. A material, such as copper or aluminum, with a large thermal conductivity, κ, dissipates heat quickly, while one with a low thermal

conductivity, such as glass and plastic, dissipate heat more slowly, and thus heat up and damage more easily. The absorption coefficient, α, is another key property, which, not surprisingly, varies with wavelength. It can be calculated by multiplying the imaginary component of the refractive index by 4π/λ. The higher the absorption coefficient, the lower the damage threshold.

Regarding the compositions, AMTIR-1 and IRG-24 are both GeAsSe compositions; IRG-26 is GeSbSe, AMTIR-6 and IRG-27 are both AsS; while the remaining are AsSe compositions. For the Amorphous Materials Inc AsSe compositions we do not know the exact composition; however, we do know that the amount of As decreases from AMTIR-2 to AMTIR-5 to AMTIR-7 with AMTIR-4 having the least As (and most Se).

The transmission spectra of all Amorphous Materials Inc samples are shown in Fig. 1. The transmission spectra of the SCHOTT materials can be found on their website (SCHOTT 2018).

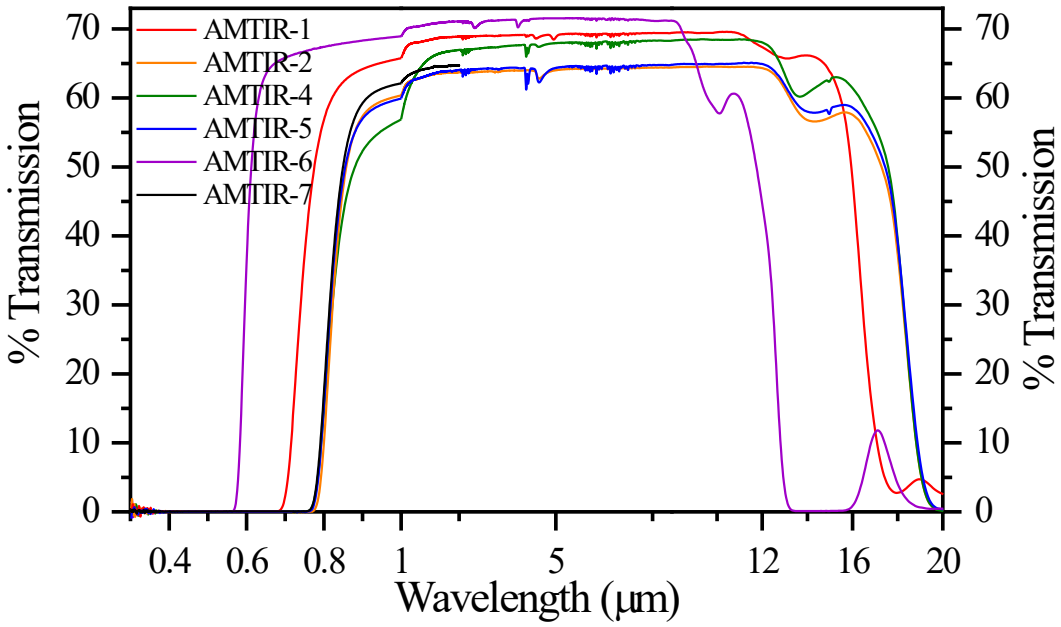

Fig. 1 Transmission spectra of chalcogenide glasses

3. Standards, Calculations, Simulations, and Setup

3.1 Standards and Parameters

The CW LIDT measurements follow International Organization for Standardization (ISO) 11254 and 21254 as closely as possible (ISO 2011a, 2011b). The standards suggest that the beam diameter remain 800 μm or larger but requires

that the spot size of the beam be larger than 200 μm. Specifically, they recommend remaining larger than 800 μm, but "the beam diameter may be reduced, depending on the power density necessary, but not to a value less than 200 μm." The lasers used for the damage testing were a 1-kW IPG laser, model YLR-1000-WC-Y11, and a 1.5 kW IPG laser, model YLR-1500-WC-Y17, which have a numerical aperture of 0.05 and a 20-μm-thick quartz block on the tip. A 35-mm focal length lens collimated the beam to approximately 3.5 mm, requiring us to use a rather long focal length lens to keep the beam larger than 200 μm. Using a 2000-mm lens to focus, the spot size of the beam on sample was kept to a $1/e^2$ diameter of 830 and 1044 μm, respectively, resulting in an effective beam diameter, $d_{T,eff}$, of 587 and 738 μm, respectively,

$$d_{T,eff} = 2\sqrt{\frac{P}{\pi E_{max}}} = 2\sqrt{\frac{A_{T,eff}}{\pi}} = 2\sqrt{\frac{\frac{1}{8}\pi d_\sigma^2}{\pi}} = \frac{1}{\sqrt{2}} d_\sigma = \frac{1}{\sqrt{2}} d_{86.5} \qquad (1)$$

where P is the total power, $A_{T,eff}$ is the effective area, and E_{max} is the maximum power. The effective diameter $d_{t,eff}$, is needed to calculate the linear power density (LPD), D_t, which has units of W/cm and is the unit of measurement used for CW damage according to the standards; it is given by

$$D_t \propto \frac{2\pi \Delta T \rho C_p D}{\alpha}. \qquad (2)$$

According to the standards and Ristau (2014), CW damage varies linearly with the spot diameter rather than area; as such, it is reported in terms of the LPD instead of the irradiance, though the spot size must also be reported (Wood 2003). This is important because many in industry, academia, and government, often report CW damage in terms of irradiance, not LPD. However, it has recently been shown by Slinker et al. (2019) that, in at least one special case, the case of a very large spot size on a thin optic, the damage threshold is constant in irradiance, not LPD. The use of effective beam diameter accounts for the Gaussian nature of the beam. For a non-Gaussian beam, the equation for the effective diameter is not the one shown in Eq. 1.

In these measurements, without clear guidance from ISO standards and staying consistent with Comer's (2016) CW LIDT measurements at longer wavelengths, the CW light is focused onto the sample for 5-s intervals to determine the damage threshold. Note that 5 s is the maximum time a spot on the sample is exposed. As soon as a spot begins to show signs of damage, the laser is manually turned off to reduce further damage to the whole sample.

3.2 Calculations

A rough estimate of the CW LIDT is calculated using the following equation (Comer 2016):

$$D_t \propto \frac{2\pi\Delta T \rho C_p D}{\alpha} \tag{3}$$

where,

ΔT = difference between room temperature and transition temperature (°C),

P = material density (g/cm^3),

C_p = specific heat (J/g °C),

D_t = thermal diffusivity (cm^2/s) = $\kappa/\rho C_p$,

α = absorption coefficient (cm^{-1}),

κ = thermal conductivity (W/cm °C).

Looking at Eq. 3, we can see that the damage threshold for an optic exposed to CW light decreases with an increase in the absorption coefficient (at the wavelength of the incident light). Likewise, the lower the glass-transition temperature, density, thermal diffusivity, or thermal conductivity, the lower the damage threshold; the thickness of the optic is not considered.

In Table 2, we see that the AMTIR-1, AMTIR-6, and IRG-27 materials should have the highest damage threshold, while the IRG-25 and IRG-26 materials should have the lowest. These calculations, combined with the simulation results, are used to give us a rough idea of the powers or linear power density at which we expect the optics to be damaged when we begin testing in the lab.

Table 2 Estimated damage threshold for different chalcogenides calculated for LPD and converted to power and irradiance for an effective diameter of 587 µm

MATERIAL	D_T (W/CM)		
	Power (W)	LPD (W/cm)	I (kW/cm^2)
IRG-24	3.1	52	1.1
IRG-25	1.2	20	0.4
IRG-26	1.2	20	0.4
IRG-27	7.5	127	2.8
AMTIR-1	23	391	8.5
AMTIR-2	3.2	55	1.2
AMTIR-4	4.3	74	1.6
AMTIR-5	3.6	62	1.3
AMTIR-6	9.7	165	3.6
AMTIR-7	2.0	34	0.7

3.3 Simulations

3.3.1 Motivation

As previously discussed, it is believed that the CW LIDT scales with LPD. For these measurements, all samples are being tested with a small spot size with a diameter between 800 and 1100 μm. For the results we obtain to be useful at larger diameters, we need to have confidence that the threshold values scale with the LPD. Our approach, and ultimate goal, is to model these laser and optical interactions, validate them with experimental results, and further modify the model until it matches the experiment. Though we have not yet achieved that here, the next step would be to test a number of samples at larger spot sizes to confirm that the simulations match. If we could achieve this, not only would it allow us to be confident in scaling our damage results to more realistic spot sizes, which may be encountered outside of a lab setting, but it would also allow us to determine the CW LIDT of optics that we have not yet measured.

In this report, we use the simulations to get a feel for where the damage threshold will be and the overall trends, and to analyze our data. As we have not yet fully fine-tuned the model, we will only briefly present our findings with a few examples and summarize results, instead of going into detail for all of our simulations on each different chalcogenide.

3.3.2 Model

The temperature distribution resulting from the laser absorption is modeled by solving two partial differential equations: one for the absorption of light and the other for the heat flow.

The intensity is modeled by the Beer–Lambert law, where the beam is assumed to propagate in the z direction and intensity I is given by

$$\frac{\delta I(r,z,t)}{\delta z} = -\alpha I(r,z,t) \tag{4}$$

where z is the coordinate along the beam direction, and α is the absorption coefficient of the material. At wavelengths around 1 μm, the absorption coefficient of chalcogenide glass has a very weak temperature dependence; therefore, the absorption coefficient is assumed to be a constant (Nguyen 1999).

We also solve the governing partial differential equation for temperature distribution within the material,

$$\rho C_p \frac{\delta T}{\delta t} - \nabla \cdot (k \nabla T) = Q = \alpha I \tag{5}$$

where the heat source term, Q, arises from the absorption of the laser light. The surface of the material is modeled with a diffuse boundary condition, which accounts for radiative heat loss using an ambient temperature of 300 K and a surface emissivity of 0.8. The diffuse surface boundary condition is valid for the re-radiation at long-IR wavelengths corresponding to the temperatures below the melting point of the material.

Simulations were run for 1.07 µm light focused down to a Gaussian spot size of either 830 µm (corresponding to an effective diameter of 587 µm) or 1044 µm (corresponding to an effective diameter of 738 µm), depending on the corresponding experimental setup. Simulations of a 3-mm-thick sample of IRG-25 were run using the parameters given in Table 1 with three different irradiances—0.9, 1.0, and 1.23 kW/cm^2—corresponding to the linear power density and power in Table 3.

Table 3 Irradiance, LPD, and power used in IRG-25 simulations

Irradiance (kW/cm^2)	LPD (W/cm)	Power (W)
0.9	38.0	2.04
1.0	42.2	2.26
1.23	51.9	2.79

Figure 2 shows a surface plot of the temperature distribution of one quadrant of the IRG-25 sample irradiated with 1 kW/cm^2, which looks as we would expect.

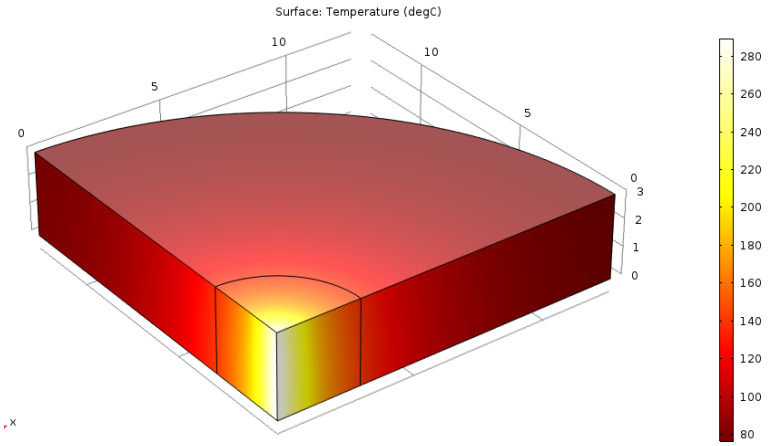

Fig. 2 Surface plot of the temperature distribution for an irradiance of 1 kW/cm^2

3.3.3 Results

Before measuring the damage thresholds in the lab, we ran two main types of simulations: the first with fixed time and varying power (either 5 s, to model the experimental conditions, or 10 min, to simulate steady state—the upper bound) and the second with fixed power and varying time. In an attempt to determine the damage threshold that we will measure in the lab with an irradiance time of 5 s, simulations were run with a 5-s irradiance time and varying power to determine at which linear power density the material would heat up to the glass-transition temperature (i.e., the temperature at which we expect damage to occur); see Table 4.

Table 1 Damage threshold estimated from simulations for a 5-s and 10-min (approximating steady state) irradiance time, assuming that damage occurs when the window heats up to the glass-transition temperature

	SIMULATION (5 S)			SIMULATION (10 MIN/STEADY STATE)		
SAMPLE	**Power (W)**	**LPD (W/cm)**	**I (kW/cm^2)**	**Power (W)**	**LPD (W/cm)**	**I (kW/cm^2)**
IRG-24	40.4	688	14.9	20.0	341	7.4
IRG-25	14.6	248	5.4	7.3	124	2.7
IRG-26	15.1	258	5.6	7.5	127	2.8
IRG-27	90.7	1230	21.2	41.1	557	9.6
AMTIR-1	57.6	982	21.3	28.1	478	10.4
AMTIR-2	34.1	581	12.6	17.4	297	6.4
AMTIR-4	47.3	806	17.5	22.0	375	8.1
AMTIR-5	43.5	741	16.1	22.1	377	8.2
AMTIR-6	161.3	2186	37.7	72	976	16.8
AMTIR-7	30.9	419	11.4	15.2	206	5.6

To determine an upper bound of damage, we also ran simulations for 10 min to approximate the steady state solutions. For IRG-26, the powers that resulted in a rise in temperature of the chalcogenide to the glass-transition temperature at 10 min, were within 1.8% of the steady state temperature.

Once the simulated damage threshold linear power densities were determined, we also ran simulations for this fixed-LPD with varying times to get a feel for how quickly and how much the optics heated up, as can be seen for IRG-25 in Fig. 3. We see that, in this case, from 5 s to 10 min, the maximum temperature of the sample nearly doubles. Also, at only 1 s, the sample has already reached a temperature over halfway to the glass-transition temperature.

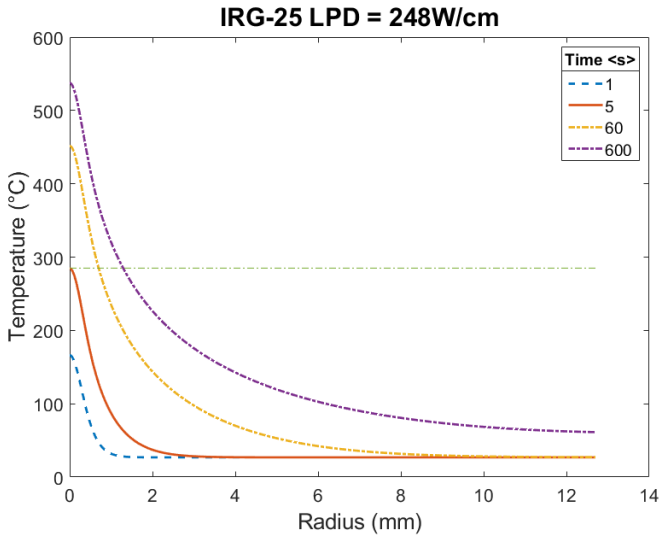

Fig. 3 Plot of temperature from the center of the IRG-25 sample to the edge for four different irradiance times with a constant LPD of 248 W/cm, the power at which the glass-transition temperature is reached after 5 s of irradiance

We can also look at the temperature distribution throughout the thickness of the samples—this one is 3 mm (Fig. 4)—to see at what depth the temperature of the chalcogenide reached the peak; for this IRG-25 sample it was around 2 mm.

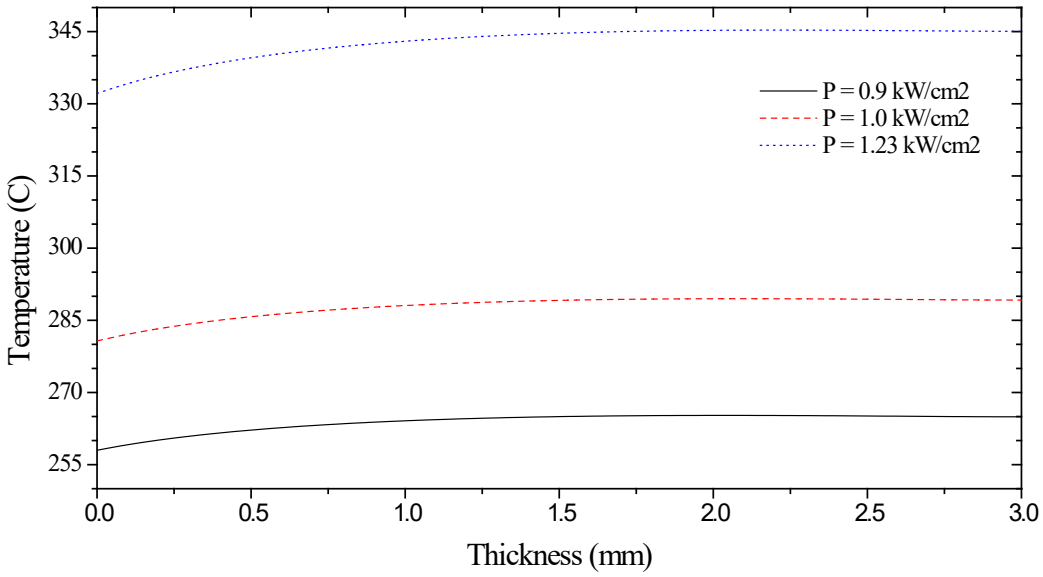

Fig. 4 Plot of the temperature along *z* at the center of the spot for three different irradiances

With preliminary simulations complete, we can move on to the experiment, then we will review simulations done using the experimental data to analyze the data and improve upon the model; see Table 5.

Table 5 The calculated and simulated linear power density CW damage threshold estimates for the ChGs under test

SAMPLE	CALC.	SIM. (5 S)	SIM. (10 MIN)
IRG-24	52	688	341
IRG-25	20.3	248	124
IRG-26	20	258	127
IRG-27	127	1230	557
AMTIR-1	391	982	478
AMTIR-2	55	581	297
AMTIR-4	74	806	375
AMTIR-5	62	741	377
AMTIR-6	165	2187	976
AMTIR-7	34	419	206

3.4 Safety Enclosure at 1 kW

All LIDT measurements were performed in the HiPo CoW Laser Laboratory for Sensors and Optics inside the Kilowatt Interlocked Light-Tight Enclosure (KILTE) (Fig. 5). The enclosure is made of 0.25-inch-thick anodized aluminum, tested with powers up to 1 kW of 1.07-µm light focused down to roughly 200 µm for up to 100 s, and framed with 1-inch aluminum t-slotted framing.

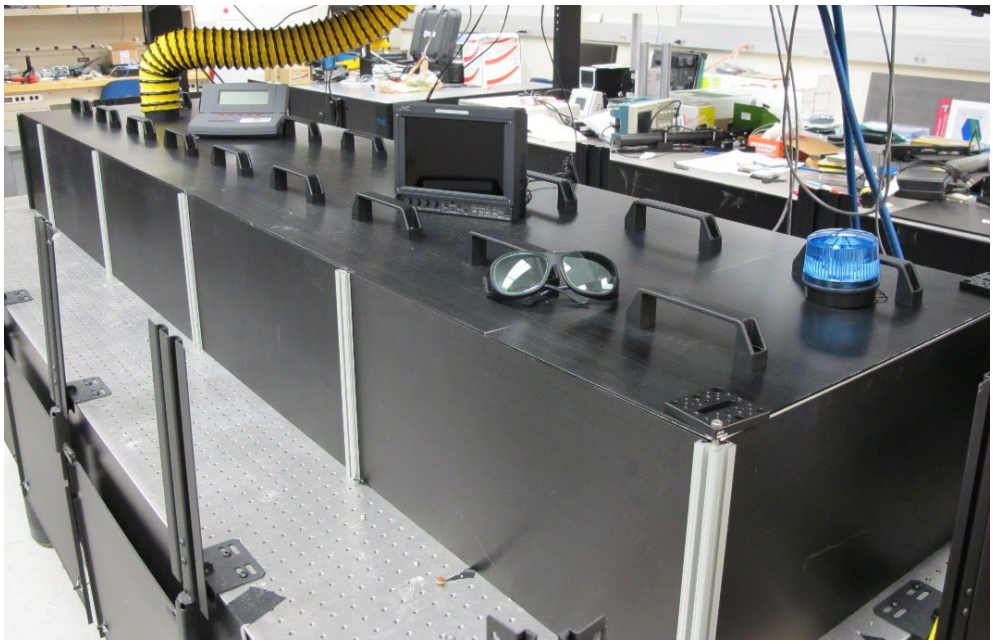

Fig. 5 KILTE

The lid panels (Fig. 6) are cut so that there is a lip over the edge of the walls and adjacent panels overlap creating robust and light-tight lids and walls.

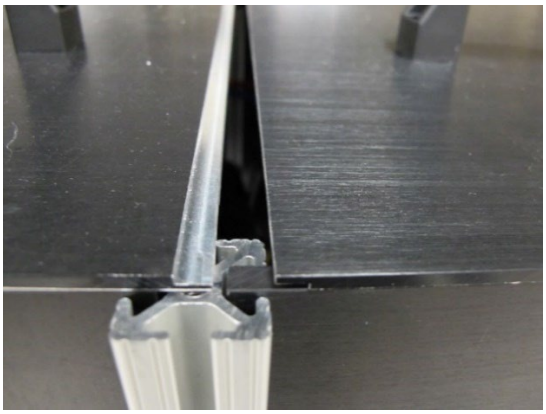

Fig. 6 Lid panels, cut to overlap and have a lip over the walls—to keep the enclosure light-tight

Wires, hoses, fibers, and all other cables enter the enclosure through a "light labyrinth" (Fig. 7)—a hole in the bottom of one of the panels enclosed on both sides by multiple 90° 0.25-inch aluminum pieces.

Each lid panel is interlocked such that if any of the panels are removed, the laser shuts off. Likewise, the laser is interlocked to the door of the lab.

Because of the thickness of the 1.5-kW IPG fiber, a modification had to be made for the insertion of the fiber.

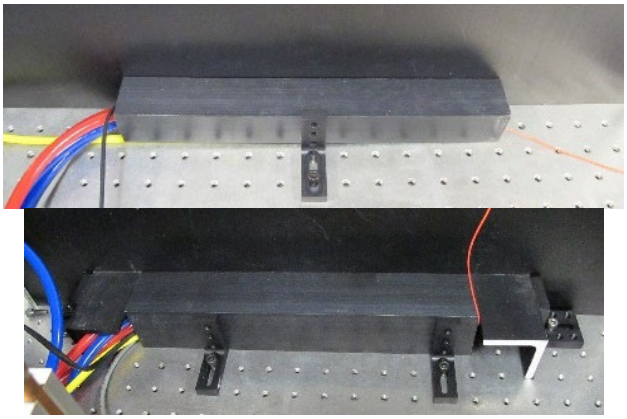

Fig. 7 Light labyrinth

3.5 Experimental Setup and Procedure

All laser-induced damage threshold measurements were performed in the HiPo CoW inside the KILTE, which houses several cameras to monitor the setup and the sample for damage. To measure the damage threshold, using the 1.07-µm, 1-kW IPG laser, the output unpolarized light was collimated and then focused using 35- and 2000-mm lenses, respectively (Fig. 8). The beam, after leaving the focusing

optics, then passes through a high-powered shutter (not shown; US Laser Corp N8022) to control the duration of the CW beam on the sample. The shutter is controlled by a circuit designed by Dr Nicholas Barbieri to keep the shutter open for precisely 5 s. For the 1-kW laser, the power is controlled further using two thin film polarizers (TFPs) separated by a half-waveplate (in the dashed box). In this setup, the first TFP dumps roughly half of the unpolarized light and thus reduces the output power significantly. For the 1.5-kW laser, the power is controlled using the computer/laser interface. The power and beam shape are monitored using two 0.05% beams diffracted from the main beam at 10° through a holographic beam sampler (Gentec HBS-1064-2000-1C-10). In later damage measurements of materials for which higher powers were necessary (>300 W), the Gentec HBS started to distort the beam on the sample causing it to spread out in the *x* (horizontal) direction and initially contract in the *y* (vertical) direction resulting in a lower LPD and irradiance as the power was further increased. The main beam proceeds to focus onto the sample under test with the transmitted light going into a high-power beam dump. The SCHOTT IRG test samples are 3-mm thick with a 1-inch diameter, while the Amorphous Materials Inc samples are 2-mm thick also with a 1-inch diameter. The test samples are angled slightly with the reflected beam directed to a beam dump (not shown). A camera is used to monitor the onset of damage. There is an exhaust port a few inches above the sample; it has been reported that any airflow over the sample may alter the damage threshold. However, we have not explored such effects ourselves.

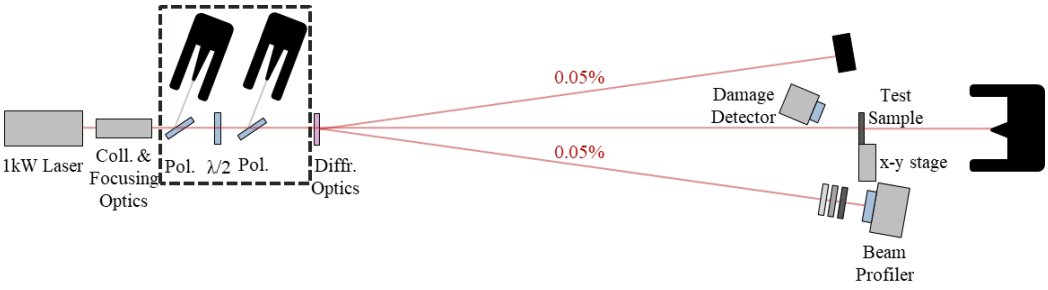

Fig. 8 Experimental setup used to measure the CW LIDT

An initial sample is used to determine a rough LPD required to damage the sample. Initial measurements are performed at a power level slightly lower than the power corresponding to the LIDT estimated through calculations and simulations. The power is then increased, on the same spot, until damage occurs. These initial measurements are made for various times. Once we get consistent damage at a few spots, we reduce the irradiance time down to 5 s, readjust the power to get damage, and proceed.

Once a rough damage threshold is established, repeat measurements are performed on subsequent rows at or near this power level starting from powers below the threshold. For each power, the beam is focused onto 10 different untested spots before proceeding to higher powers. This is repeated until a power level is reached at which the sample is damaged for all 10 runs. This is then repeated at least once more for a power beyond that for which damage occurred during all 10 runs. When necessary, for a more thoroughly fleshed out threshold curve, the sample is tested for powers between that for which no damage occurred and for which damage occurred on each run.

For each power level, a power meter is placed in the direct beam path before and after each full run. The 5-s window is not long enough for the thermal power sensor to give a stable reading for each shot. A spot on the sample is exposed for a *maximum* of 5 s. As soon as a spot begins to show signs of damage, the laser is manually turned off. If the sample cracks, it is important to avoid testing for damage in close vicinity to the cracks. Cracks cannot always easily be seen on the surface but become apparent once the laser is turned on from the image seen on the camera without an IR filter (Fig. 9).

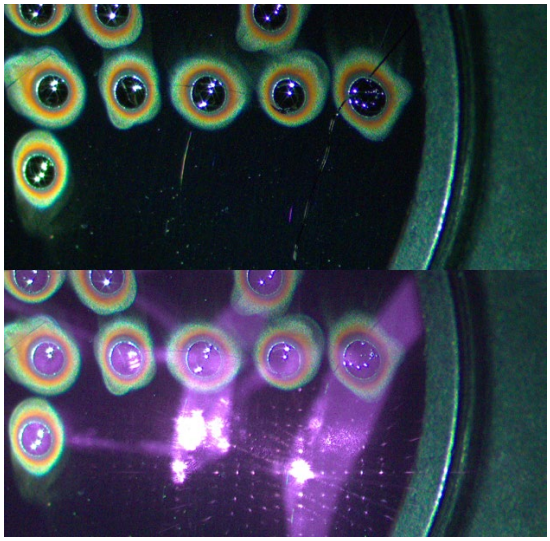

Fig. 1 IRG-26 sample 10 image from a camera with (top) and without (bottom) an IR filter and 1-µm laser irradiating the optic

The highest LPD at which there is zero probability of damage, D_t, is the CW LIDT of the material. Though not mentioned in the standards, we have included a figure, $D_{t,90}$, which is the LPD at which there is a 90% chance of damage occurring. The damage threshold is an incredibly useful value to know, especially when designing a system, as it reveals if damage *may* occur; however, $D_{t,90}$ is a useful figure to determine if damage is likely to occur in a system.

Though microscopy was never needed to determine if damage occurred in the testing of these chalcogenide samples, Nomarski microscopy was still used to get a better visual of damage to the optic. While most of the chalcogenide samples were non-transmissive in the visible (the exception being AsS compositions IRG-27 and AMTIR-6), reflected light differential interference contrast (DIC) microscopy and bright-field illumination were used. Reflective DIC, much like a scanning electron microscope, provides a topological analysis of the optic.

4. Measurement Results

Measurements using the previously described methods were made on the commercially available SCHOTT and Amorphous Materials Inc chalcogenides detailed in Section 2. The experimental results are broken down specifically by material in the following subsections.

4.1 SCHOTT IRG-24 ($Ge_{10}As_{40}Se_{50}$)

The CW damage results for a 5-s irradiance time on SCHOTT IRG-24 are presented in Table 6. More details on the results for this and the remaining materials can be found in the Appendix. Three 1-inch-diameter, 3-mm-thick samples were tested for a range of powers with 10 runs for each individual power with an effective diameter of 587 μm (Gaussian diameter of 830 μm). The optical flats were manufactured by SCHOTT on 19 May 2016 and are melt no. 14004. All measurements were conducted 5–9 August 2019.

Table 6 Damage results for different power densities and the probability of damage

Sample no.	Linear power density (W/cm)	No damage	Damage	Probability of damage
1	67.5	5	5	0.50
1	60.9	6	4	0.40
1	50.9	8	2	0.20
1	43.0	9	1	0.10
1	34.1	. . .	. . .	. . .
2	34.2	8	2	0.20
2	25.8	9	1	0.10
2	17.8	10	0	0.00
2	77.8	7	3	0.30
2	94.5	3	7	0.70
3	111.8	2	8	0.80
3	128.4	1	9	0.90
3	144.4	0	10	1.00

The powers ranged from the highest power for which no damage occurred on any of the runs (17.8 W) to the lowest power for which damage occurred on all 10 runs (144.4 W). All damage reported was large and visible to the naked eye, as can be seen in the images for each of the three samples; see Fig. 10.

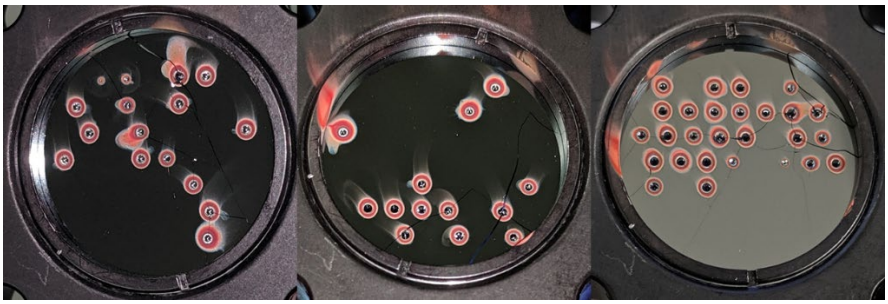

Fig. 10 Front surface of the three IRG-24 test samples after testing. Damage tests start from lower powers at the top left to higher powers at the bottom left, generally.

Plotting the data (Fig. 11) and fitting it to a linear curve, we estimate the damage threshold, D_t, for an effective diameter of 587 μm and a radiation time of 5 s, to be 5.1 W/cm, and what we call the damage threshold with 90% likelihood, $D_{t,90}$, to be 143 W/cm.

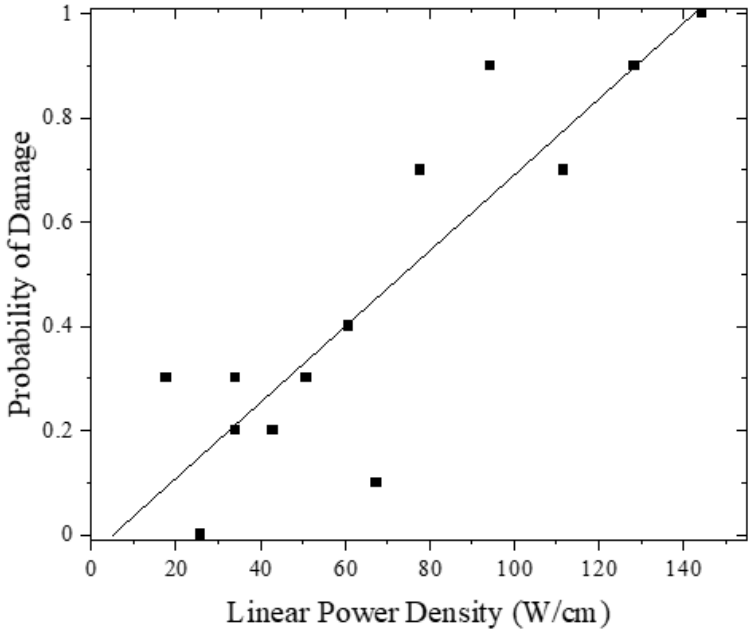

Fig. 11 Plot of the probability of damage as a function of the linear power density for the SCHOTT IRG-24 chalcogenide window for a 587-μm effective diameter beam with a 5-s radiation time. The straight line is the linear fit of the probability, while the blocks are the probability of damage for specific LPDs.

4.2 SCHOTT IRG-25 ($Ge_{28}Sb_{12}Se_{60}$)

The CW damage results for a 5-s irradiance time on SCHOTT IRG-25 are presented in Table 7. Three 1-inch-diameter, 3-mm-thick samples were tested for a range of powers with 10 runs for each individual power with an effective diameter of 587 μm (Gaussian diameter of 830 μm). The optical flats were manufactured by SCHOTT and are melt no. 1578134 and no. 14027. All measurements were conducted 18–21 May 2018.

Table 7 The damage results for different power densities and the probability of damage for IRG-25

Linear power density (W/cm)	No damage	Damage	Probability of damage
37.9	10	0	0.0
40.2	9	1	0.1
42.6	6	4	0.4
43.8	4	6	0.6
44.9	2	8	0.8
46.5	0	10	1.0

The powers ranged from the highest power for which no damage occurred on any of the runs (2.2 W) to the lowest power for which damage occurred on all 10 runs (2.7 W). All damage reported was large and visible to the naked eye, as can be seen in the images for each of the three samples; see Fig. 12.

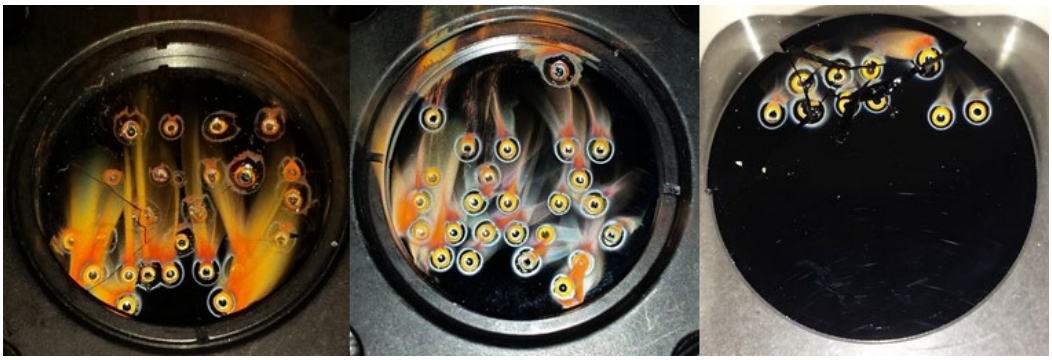

Fig. 12 Front surface of the three IRG-25 test samples after testing. Damage tests start from lower powers at the top left to higher powers at the bottom left, generally.

Plotting the data (Fig. 13) and fitting it to a linear curve, we estimate the damage threshold, D_t, for an effective diameter of 587 μm and a radiation time of 5 s, to be 39.6 W/cm, and what we call the damage threshold with 90% likelihood, $D_{t,90}$, to be 45.9 W/cm. The SCHOTT IRG-25 has a much steeper threshold curve than IRG-24.

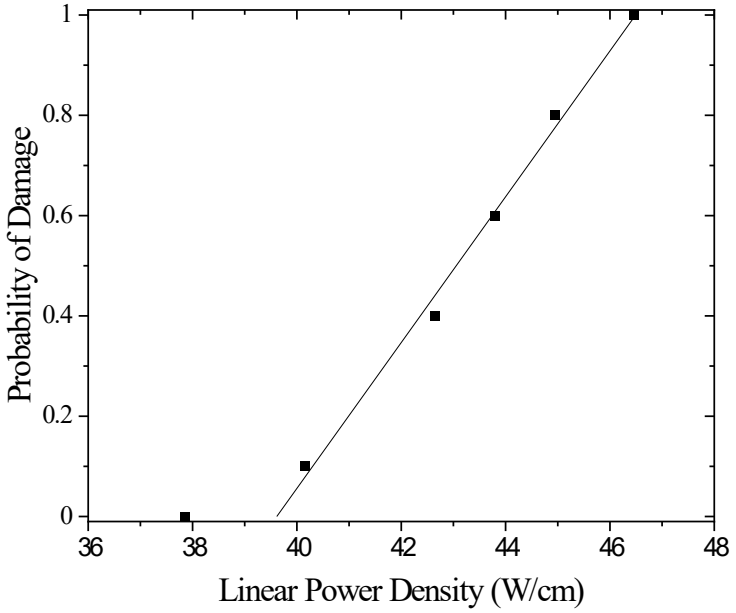

Fig. 13 Plot of the probability of damage as a function of the LPD for the SCHOTT IRG-25 window for a 587-µm effective diameter beam with a 5-s radiation time. The straight line is the linear fit of the probability, while the blocks are the probability of damage for specific LPDs.

4.3 SCHOTT IRG-26 ($As_{40}Se_{60}$)

The CW damage results for a 5-s irradiance time on SCHOTT IRG-26 (composition $As_{40}Se_{60}$) are presented in Table 8. Three 1-inch-diameter, 3-mm-thick samples were tested for a range of powers with 10 runs for each individual power with an effective diameter of 587 µm (Gaussian diameter of 830 µm). Two different sets of samples were used for these measurements. The first set, samples 1–7, were manufactured by SCHOTT on 15 March 2016 (glass no. 1578133 and melt no. 14048) and were tested 18 June–19 December 2018. The second set, samples 8–11, were manufactured on 15 May 2018 (batch no. 17133) and were tested on 20 and 21 December 2018.

Table 8 Damage results for different power densities and the probability of damage for IRG-26

Sample no.	Linear power density (W/cm)	No damage	Damage	Probability of damage
1	106.6	9	1	0.10
1	102.2	9	1	0.10
1	97.2	9	1	0.10
1	90.5	7	3	0.30
1	85.2	10	0	0.00
2	89.9	8	2	0.20
2	96.3	7	3	0.30
3	102.0	8	2	0.20
3	112.0	9	1	0.10
3	123.1	1	9	0.90
4	115.8	3	7	0.70
4	115.3	4	6	0.60
4	112.4	5	5	0.50
5	106.7	9	1	0.10
5	107.8	8	2	0.20
5	102.1	10	0	0.00
6	127.2	1	9	0.90
6	133.6	0	10	1.00
7	83.8	9	1	0.10
7	93.7	8	2	0.20
7	100.6	7	3	0.30
7	111.6	4	6	0.60
8	106.2	8	2	0.20
8	111.9	9	1	0.10
8	117.5	8	2	0.20
8	126.0	6	4	0.40
9	136.3	10	0	0.00
9	145.5	3	7	0.70
9	151.8	4	6	0.60
9	159.0	2	8	0.80
10	164.1	0	10	1.00
10	152.2	4	6	0.60
10	145.2	3	7	0.70
11	135.7	6	4	0.40
11	135.9	7	3	0.30
11	93.9	10	0	0.00
11	103.2	10	0	0.00
11	110.2	9	1	0.10

The powers ranged from the highest power for which no damage occurred on any of the runs (9.6 W) to the lowest power for which damage occurred on all 10 runs (4.9 W). All damage reported was large and visible to the naked eye, as can be seen in the images for 10 of the samples; see Figs. 14 and 15.

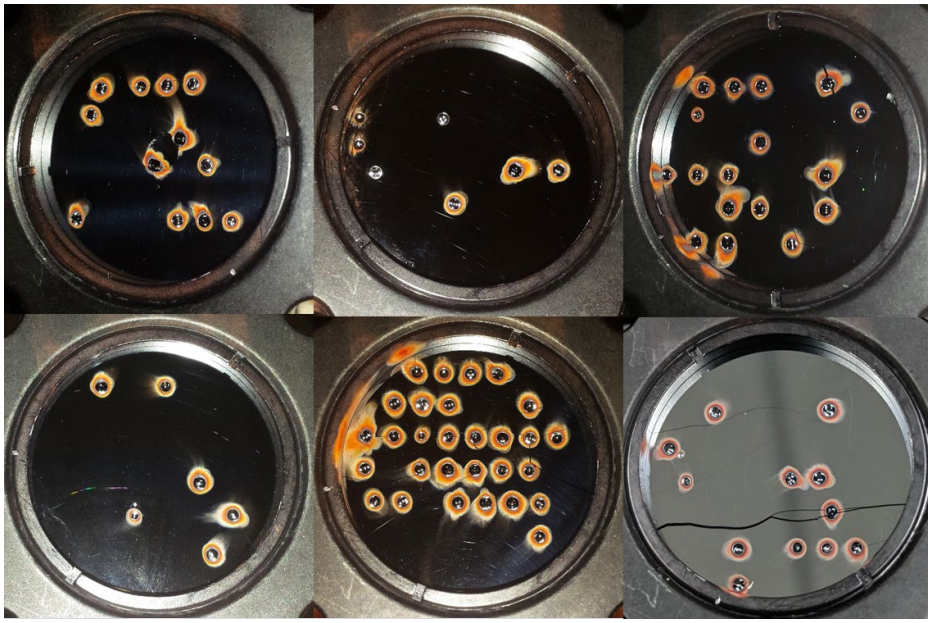

Fig. 14 The front surface of the first batch of IRG-26 test samples after testing. Top row, left to right: samples 1, 2, and 4. Bottom row, left to right: samples 5–7.

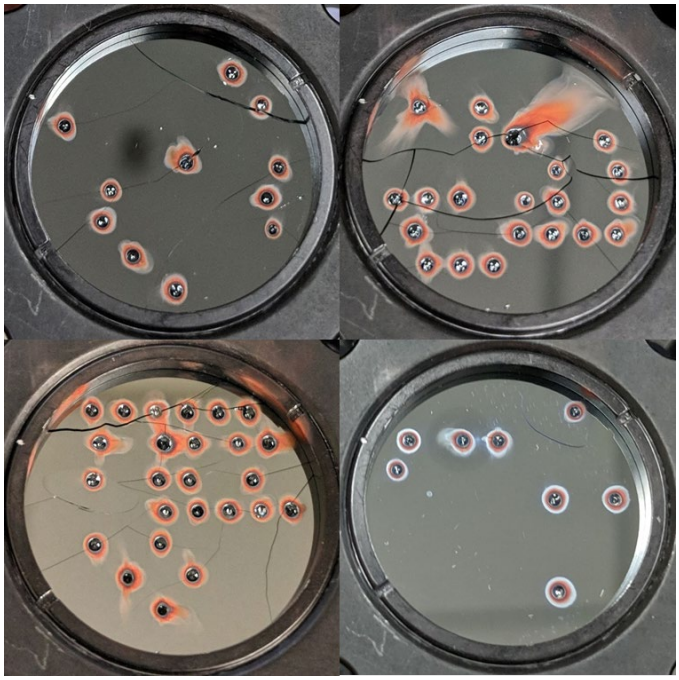

Fig. 15 The front surface of the second batch of IRG-26 test samples after testing. Top row, left to right: samples 8 and 9. Bottom row, left to right: samples 10 and 11.

Samples that look darker (more black) were captured using a flash, while those that look lighter (more gray) were captured without using a flash and show the reflection of the ceiling panels in the lab. Figure 16 shows the rear surface of samples 7 and 9 showing cracks and some burn-through spots that went completely through the sample.

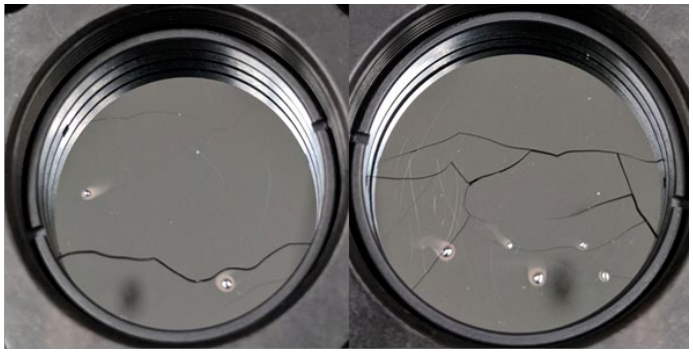

Fig. 16 Rear surface of IRG-26 samples 7 and 9

In Fig. 17, the two different batches are plotted and fitted to a linear curve separately to determine the damage threshold before fitting a linear curve to all of the data. After testing the first six samples, the results at lower powers were less consistent than at higher powers or with the IRG-25 glasses; therefore, we attained more samples of the IRG-26, which were a different batch/melt than the previous batch, for further testing. To our surprise, the resulting CW damage threshold curve (red circles) was distinctly different than with the previous batch. The lines are linear and the curve fits to batch one (black solid), batch two (red dotted), and all the data (blue-dot dashed). From the two sets of samples, the CW LIDT is broadly between 81 (overall) and 101 W/cm (batch 2), for an effective beam diameter of 587 μm, an exposure of 5 s, and a wavelength of 1.07 μm. Looking at each curve individually, each batch resulted in significantly different damage threshold curves with the first batch having a damage threshold, D_t, for an effective diameter of 587 μm and a radiation time of 5 s, 87 W/cm, and a $D_{t,90}$ of 132 W/cm. The second batch had a D_t of 102 W/cm and a $D_{t,90}$ of 180 W/cm. The average threshold is 81 W/cm with the 90% likelihood of damage being 180 W/cm.

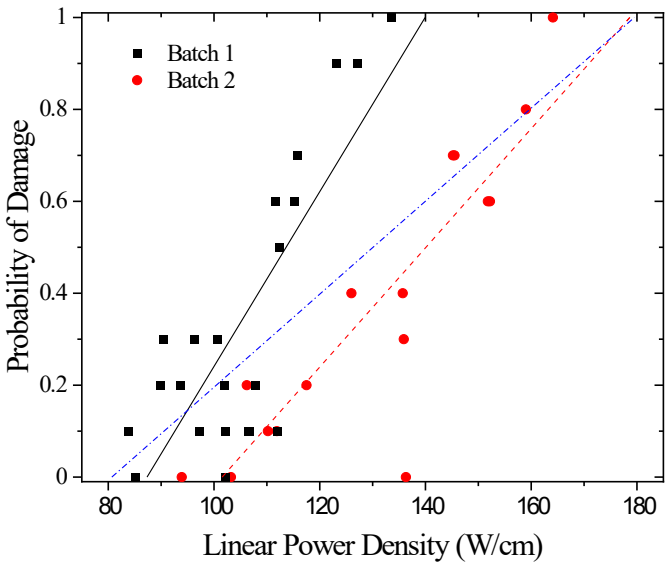

Fig. 17 Plot of the probability of damage as a function of the LPD for the SCHOTT IRG-26 window for a 587-µm effective diameter beam with a 5-s radiation time. The straight line is the linear fit of the probability, while the blocks are the probability of damage for specific LPDs.

Based on observations made in an arsenic selenide thin film by Frantz et al. (2018), the change in the damage threshold between the two batches is likely the result of degradation of the samples from exposure to light and humidity over time. Frantz et al. (2018) found that arsenic selenide thin films degraded with the formation of defects due to photo-induced crystallization with the aid of moisture and water, which produces As_2O_2 and Se crystallites. The first IRG-26 batch was produced on 15 March 2016 and was tested June–August 2018 (over 2-years apart), while the second batch was produced on 15 May 2018 and tested in December 2018 (~7 months apart). Assuming the observations made for the AsSe thin film hold true for the bulk material, our results seem to indicate that as the sample was exposed to humidity and/or light, the resulting damage threshold decreased, which must be considered with any measurements made or used. Further studies would be beneficial to determine if and at what point a saturation is reached beyond which the thermal properties no longer change.

Figure 18 shows the bright- and dark-field images of a damage spot captured with a Nomarski microscope magnified by a factor of 20. This is the only damage spot of all the chalcogenides tested, which displays the initial stage of damage on a chalcogenide optic from a CW laser. The sample had just begun to damage as the 5-s shutter was closing.

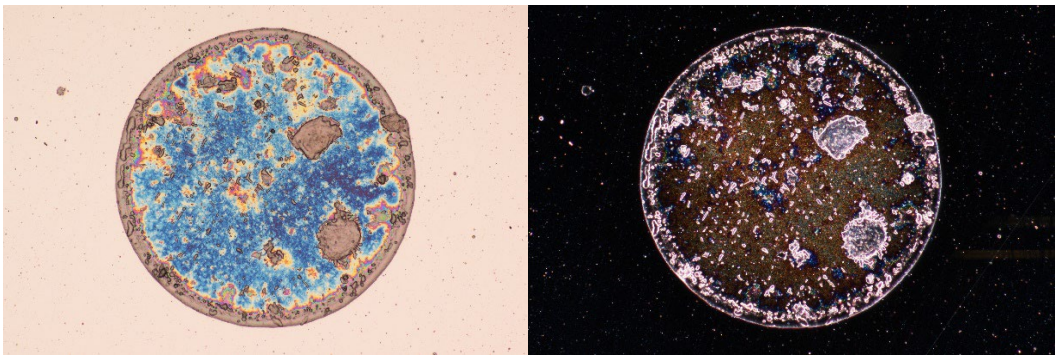

Fig. 18 Damage spot from sample 11 (center left on the sample). This is the only damage spot in any of the chalcogenides that started just as the shutter was closing. It shows us the very initial stage of damage on a chalcogenide due to CW laser exposure.

4.4 SCHOTT IRG-27 (As_2S_3)

The CW damage results for a 5-s irradiance time on SCHOTT IRG-27 (composition As_2S_3) are presented in Table 9. Three 1-inch-diameter, 3-mm-thick samples were tested for a range of powers with 10 runs for each individual power with an effective diameter of 738 µm (Gaussian diameter of 1044 µm), which is a larger spot size than used on previous SCHOTT ChGs tested. The optical flats were manufactured by SCHOTT on 27 June 2018 and are melt no. 18002. All measurements were conducted 14–21 April 2021.

Table 9 Damage results for different power densities and the probability of damage for IRG-27. Note that the LPD is presented in terms of kW/cm, not W/cm.

Sample no.	Linear power density (kW/cm)	No damage	Damage	Probability of damage
1	2.23	8	2	0.20
1	1.95	10	0	0.00
1	1.73	9	1	0.10
2	1.73	10	0	0.00
2	2.64	3	7	0.70
3	3.10	2	8	0.80
3	3.57	0	10	1.00
4	3.32	1	9	0.90
4	3.79	1	9	0.90
5	1.52	10	0	0.00
5	2.43	4	6	0.60
6	3.78	0	10	1.00
7	4.01	0	10	1.00

The powers ranged from a power below the highest power for which no damage occurred on any of the runs (112 W) to a power above the lowest power for which damage occurred on all 10 runs (296 W). All damage reported was large and visible to the naked eye, as can be seen in the images for each of the six samples; see Figs. 19–21. Since the debris field around the damage spots was larger than the previously tested chalcogenides, more space was sometimes left between test spots and rows.

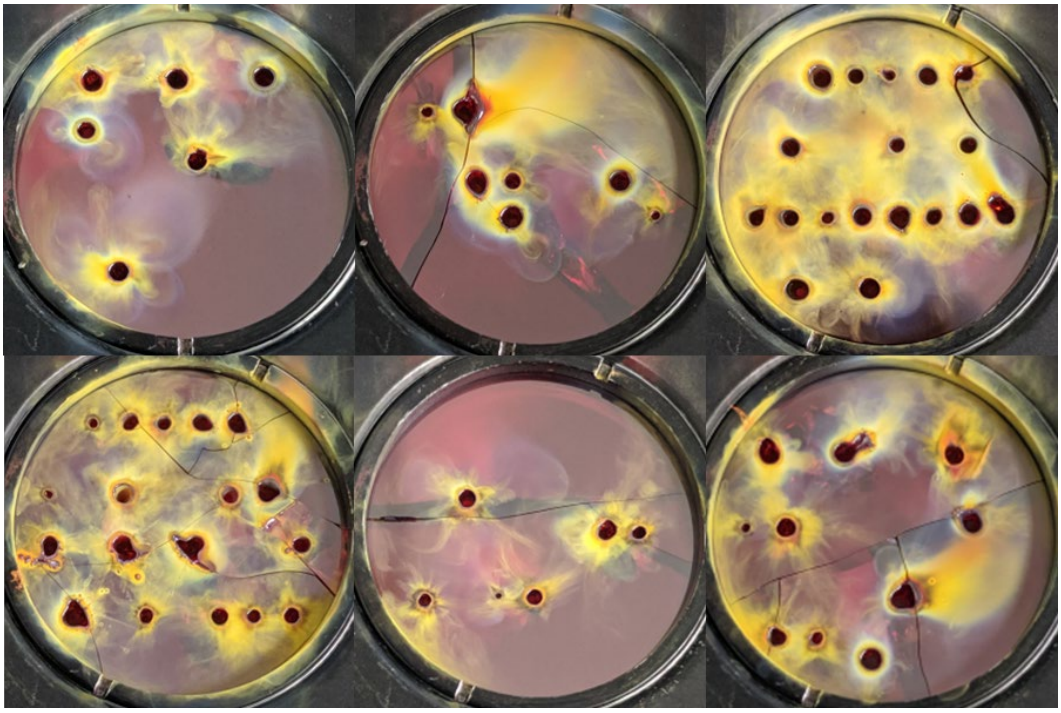

Fig. 19 Front surface of the first six of the IRG-27 test samples after testing. Images were taken without a flash.

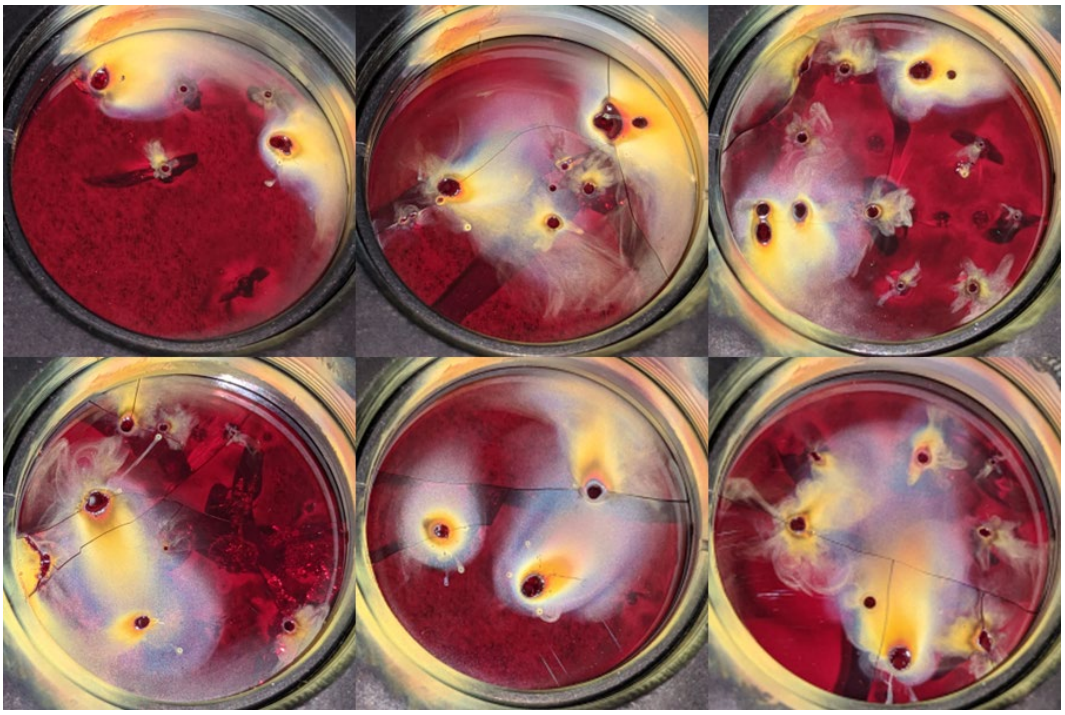

Fig. 20 Back surface of the first six of the IRG-27 test samples after testing. Images were taken with a flash.

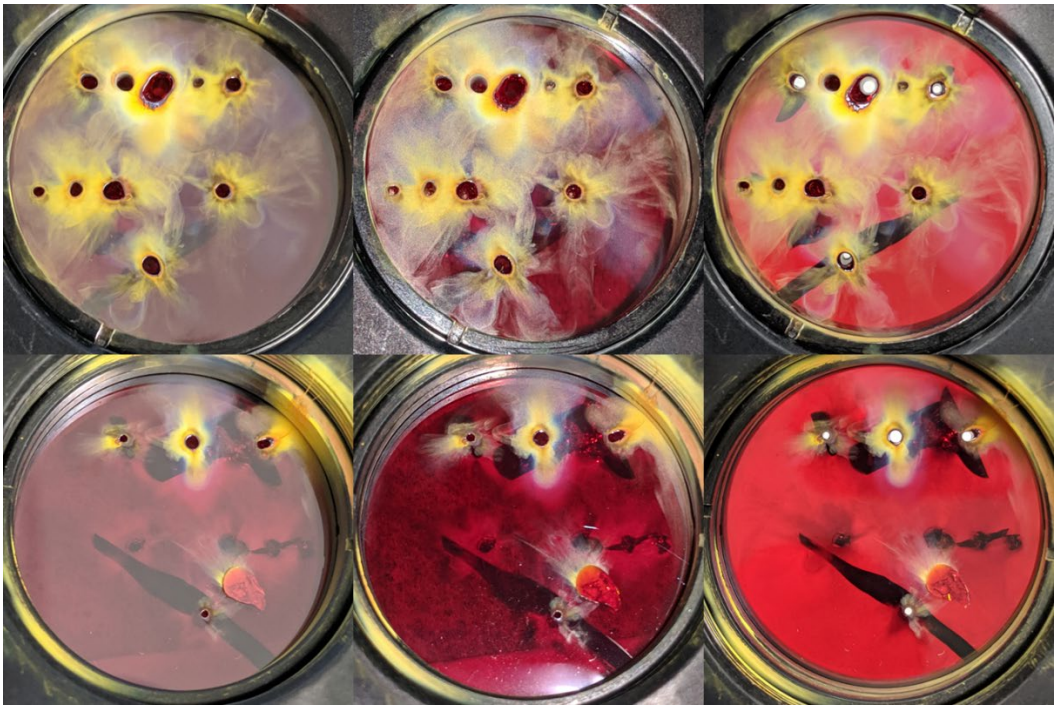

Fig. 21 Front (top row) and back (bottom row) surface of IRG-27 test sample 7 after testing recorded without a flash (left column), with a flash (middle), and with backlighting (right)

In Fig. 21, photographs of the IRG-27 taken with backlighting reveal the cracks in the sample. It can also be seen that, not surprisingly, the damage hole is smaller at the rear face of the sample than at the front face. One of the damage spots, from the back of IRG-27 sample 1, as seen in Fig. 22, was imaged with a magnification factor of 5.

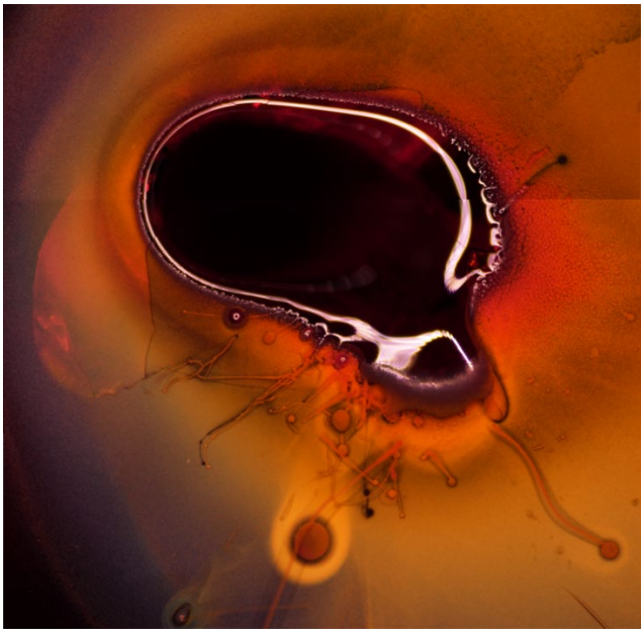

Fig. 22 Damage spot on the back of IRG-27 sample 1 magnified by a factor of 5 using reflected light dark-field illumination

Plotting the data (Fig. 23) and fitting it to a linear curve, we estimate the damage threshold, D_t, for an effective diameter of 738 μm and a radiation time of 5 s, to be 1.54 kW/cm, and what we call the damage threshold with 90% likelihood, $D_{t,90}$, to be 3.73 kW/cm. The damage threshold here is in terms of kilowatts per centimeter, not watts per centimeter as with the previous chalcogenides; therefore, the damage threshold is significantly higher for this AsS composition than the previously tested chalcogenides.

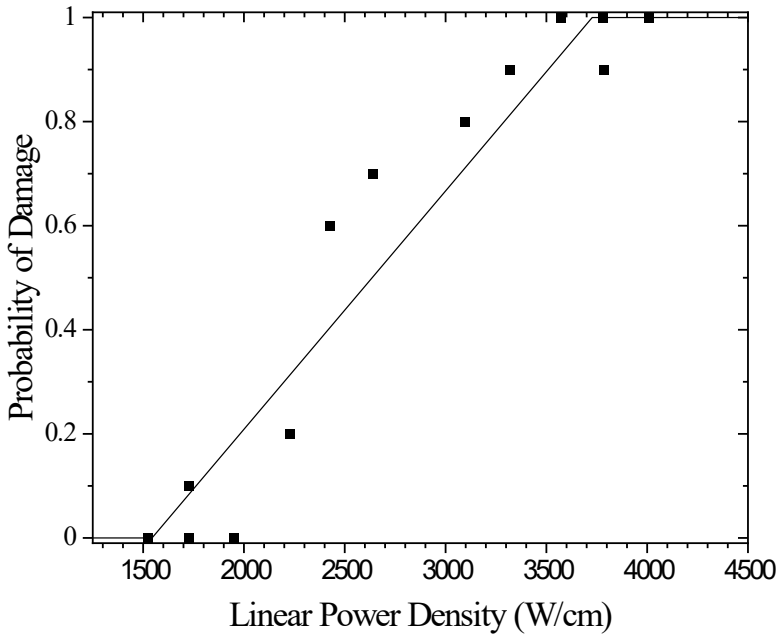

Fig. 23 Plot of the probability of damage as a function of the LPD for the SCHOTT IRG-27 window for a 738-µm effective diameter beam with a 5-s radiation time. The straight line is the linear fit of the probability, while the blocks are the probability of damage for specific LPDs.

4.5 Amorphous Materials Inc AMTIR-1 ($Ge_{33}As_{12}Se_{55}$)

Moving on to the Amorphous Materials Inc chalcogenides, we start with AMTIR-1, which has a ternary composition of $Ge_{33}As_{12}Se_{55}$. The CW damage results for a 5-s irradiance time on the optics are presented in Table 10. Three 1-inch-diameter, 2-mm-thick samples were tested for a range of powers with 10 runs for each individual power with an effective diameter of 587 µm (Gaussian diameter of 830 µm). The optical flats were manufactured by Amorphous Materials Inc, shipped on 22 February 2019, and are melt no. 18-A1-15. All measurements were conducted on 29 November 2019.

Table 10 Damage results for different power densities and the probability of damage for AMTIR-1

Sample no.	Linear power density (W/cm)	No damage	Damage	Probability of damage
1	162.4	7	3	0.30
1	140.0	10	0	0.00
1	151.6	10	0	0.00
1	174.3	7	3	0.30
1	185.3	7	3	0.30
2	195.4	6	4	0.40
2	219.8	0	10	1.00
2	208.6	0	10	1.00
2	203.7	3	7	0.70
2	161.9	7	3	0.30
3	156.4	9	1	0.10

The powers ranged from a power below the highest power for which no damage occurred on any of the runs (8.2 W) to a power above the lowest power for which damage occurred on all 10 runs (12.9 W). All damage reported was large and visible to the naked eye, as can be seen in the images of two of the samples; see Fig. 24. Being a thinner optic than the previously tested SCHOTT ChGs (i.e., 2 mm instead of 3 mm), damage on the back surface of the samples is more common with these optics.

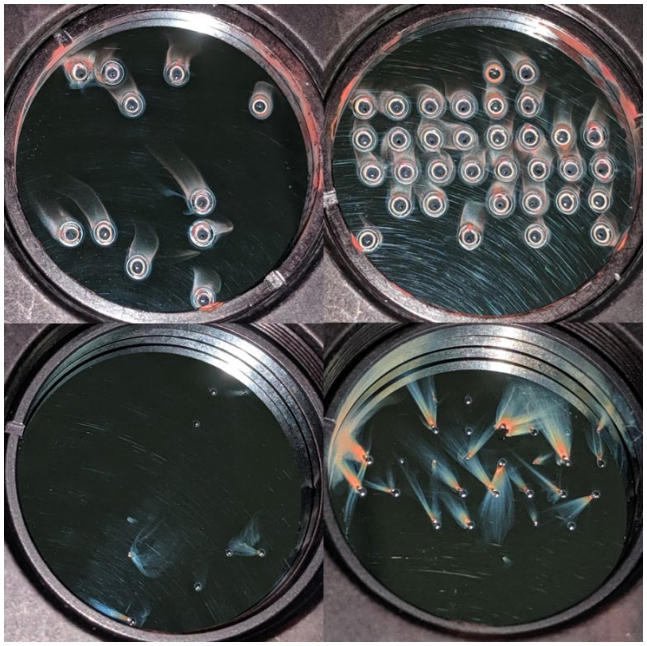

Fig. 24 Top row: Front surface of two of the AMTIR-1 test samples after testing. Bottom row: Back surface of two of the samples after testing. All photographs taken using a flash.

Plotting the data (Fig. 25), we see that, unlike in the previous damage threshold curves, there is a plateau over a range of LPDs once the probability reaches 30%. We estimate the damage threshold, D_t, for an effective diameter of 738 μm and a radiation time of 5 s, to be 153 W/cm, and the damage threshold with 90% likelihood, $D_{t,90}$, to be 208 W/cm.

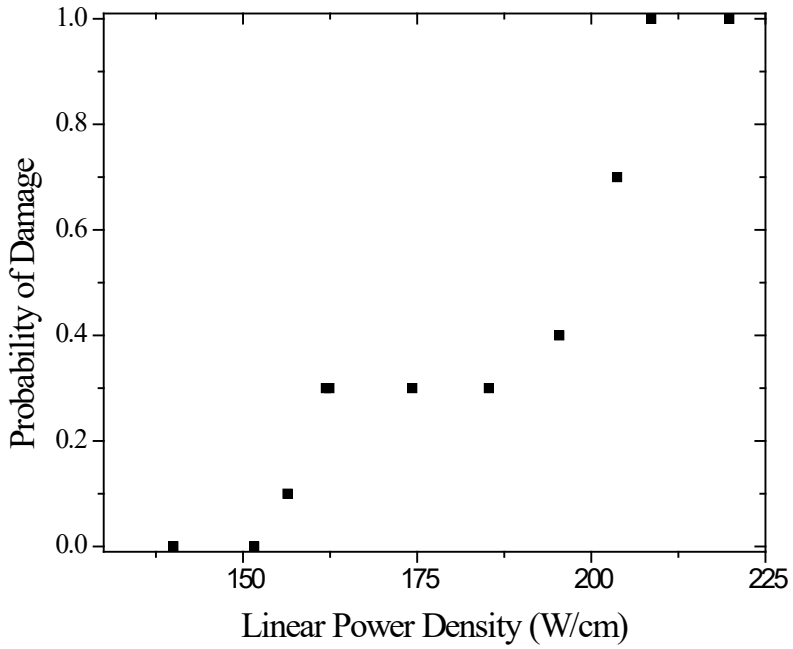

Fig. 25 Plot of the probability of damage as a function of the LPD for the Amorphous Materials Inc AMTIR-1 window for a 587-μm effective diameter beam with a 5-s radiation time. The straight line is the linear fit of the probability, while the blocks are the probability of damage for specific LPDs.

4.6 Amorphous Materials Inc AMTIR-2 (AsSe)

The CW damage results for a 5-s irradiance time on Amorphous Materials Inc AMTIR-2 (composed of AsSe) are presented in Table 11. Three 1-inch-diameter, 2-mm-thick samples were tested for a range of powers with 10 runs for each individual power with an effective diameter of 587 μm (Gaussian diameter of 830 μm). The optical flats were manufactured by Amorphous Materials Inc, shipped on 22 February 2019, and are melt no. 18-C2-3. All measurements were conducted on 9 August 2019.

Table 11 Damage results for different power densities and the probability of damage for AMTIR-2

Sample no.	Linear power density (W/cm)	No damage	Damage	Probability of damage
1	68.4	10	0	0.00
1	102.3	10	0	0.00
1	135.9	10	0	0.00
1	239.3	8	2	0.20
1	273.4	0	10	1.00
2	253.7	5	5	0.50
2	246.8	8	2	0.20
2	264.6	0	10	1.00
2	259.8	0	10	1.00
3	255.4	0	10	1.00
3	252.6	4	6	0.60
3	248.1	8	2	0.20
3	230.6	10	0	0.00
3	234.8	8	2	0.20

The powers ranged from a power below the highest power for which no damage occurred on any of the runs (4 W) to a power above the lowest power for which damage occurred on all 10 runs (16 W). All damage reported was large and visible to the naked eye, as can be seen in the images for each of the three samples; see Fig. 26. For most of the damage test spots, the laser burned through to the back of the sample, similar to the AMTIR-1, but a little more pronounced.

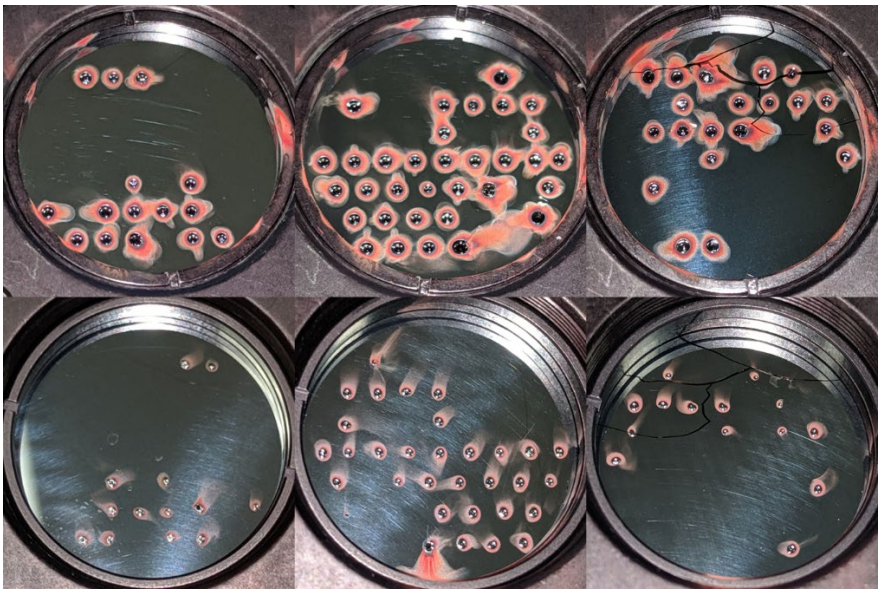

Fig. 26 Top row: Front surface of the three AMTIR-2 test samples after testing. Bottom row: Back surface of the three samples after testing.

Plotting the data (Fig. 27), we see that, similar to the AMTIR-1 threshold curve, this one displays a plateau at 20% chance of damage. We estimate the damage threshold, D_t, for an effective diameter of 587 μm and a radiation time of 5 s, to be 230 W/cm, and the damage threshold with 90% likelihood, $D_{t,90}$, to be 255 W/cm.

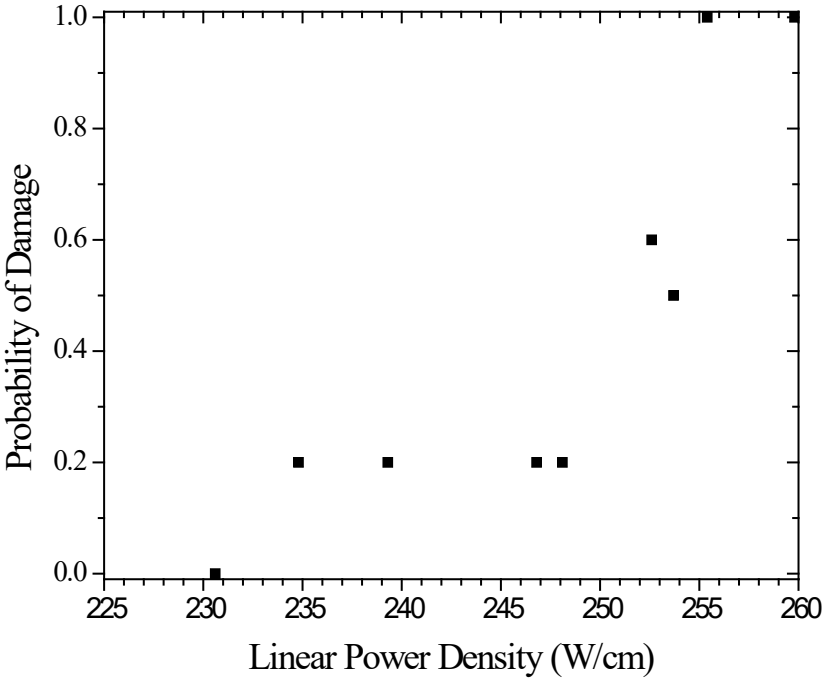

Fig. 27 Plot of the probability of damage as a function of the LPD for the Amorphous Materials Inc AMTIR-2 window for a 587-μm effective diameter beam with a 5-s radiation time. The points (all with zero probability of damage) were not included on this plot.

Figure 28 shows one of the smaller damage spots magnified by a factor of 5 with a Nomarski microscope using reflected light dark-field illumination.

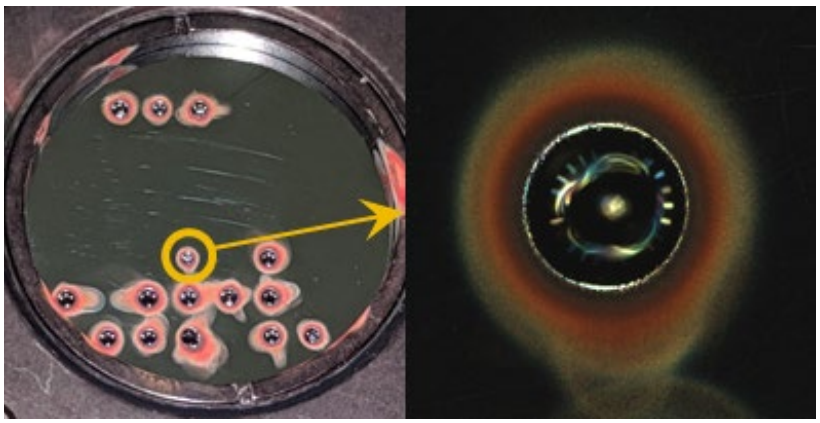

Fig. 28 Left: AMTIR-2 sample 1. Right: Image of damage spot taken with a Nomarski microscope using reflected light dark-field illumination with 5× magnification.

4.7 Amorphous Materials Inc AMTIR-4 (AsSe)

The CW damage results for a 5-s irradiance time on Amorphous Materials Inc AMTIR-4 are presented in Table 12. Six 1-inch-diameter, 2-mm-thick samples were tested for a range of powers with 10 runs for each individual power with an effective diameter of 738 μm (Gaussian diameter of 1044 μm). The optical flats were manufactured by Amorphous Materials Inc, shipped on 22 February 2019, and are melt no. 18-C4-2. All measurements were conducted on 10 August 2020.

Table 12 Damage results for different power densities and the probability of damage for AMTIR-4

Sample no.	Linear power density (W/cm)	No damage	Damage	Probability of damage
2	365.9	10	0	0.00
2	380.1	10	0	0.00
2	397.0	10	0	0.00
2	427.5	8	2	0.20
3	429.9	8	2	0.20
3	448.5	9	1	0.10
3	466.8	8	2	0.20
3	478.7	1	5	0.83
4	479.0	0	10	1.00
4	467.8	0	10	1.00
4	450.5	1	9	0.90
4	430.9	8	2	0.20
5	432.2	10	0	0.00
5	447.8	6	4	0.40
5	466.1	4	6	0.60
5	464.8	6	2	0.25
6	463.4	7	3	0.30
6	482.0	0	10	1.00
6	514.9	0	10	1.00
6	530.1	0	10	1.00

The powers ranged from a power below the highest power for which no damage occurred on any of the runs (27 W) to a power above the lowest power for which damage occurred on all 10 runs (39 W). All damage reported was large and visible to the naked eye, as can be seen in the images for each of the seven samples; see Fig. 29. Note that only five of the six samples tested are shown. The first sample experienced no damage at lower powers. Figure 30 shows that most of the damage spots burned through to the back of the sample, as with the previous 2-mm-thick Amorphous Materials Inc samples.

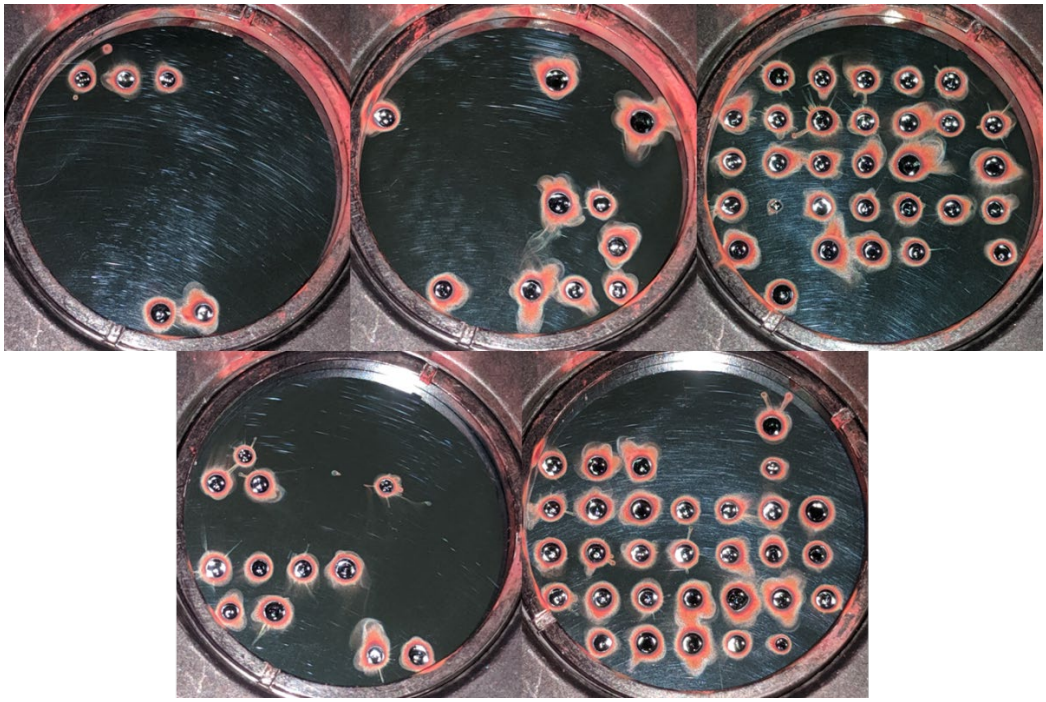

Fig. 29 Front surface of five of the AMTIR-4 test samples after testing. Samples 2 (top left) through 6 (bottom right).

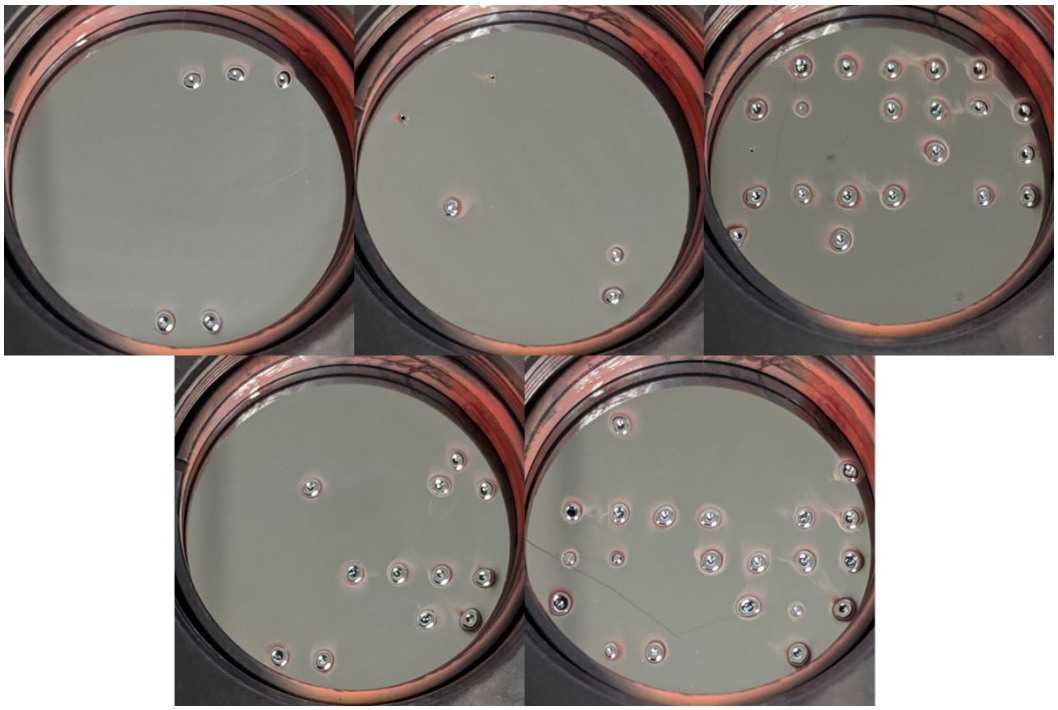

Fig. 30 Back surface of five of the AMTIR-4 test samples after testing

Plotting the data (Fig. 31) and fitting it to a linear curve, we estimate the damage threshold, D_t, for an effective diameter of 738 μm and a radiation time of 5 s, to be 413 W/cm, and the damage threshold with 90% likelihood, $D_{t,90}$, to be 491 W/cm.

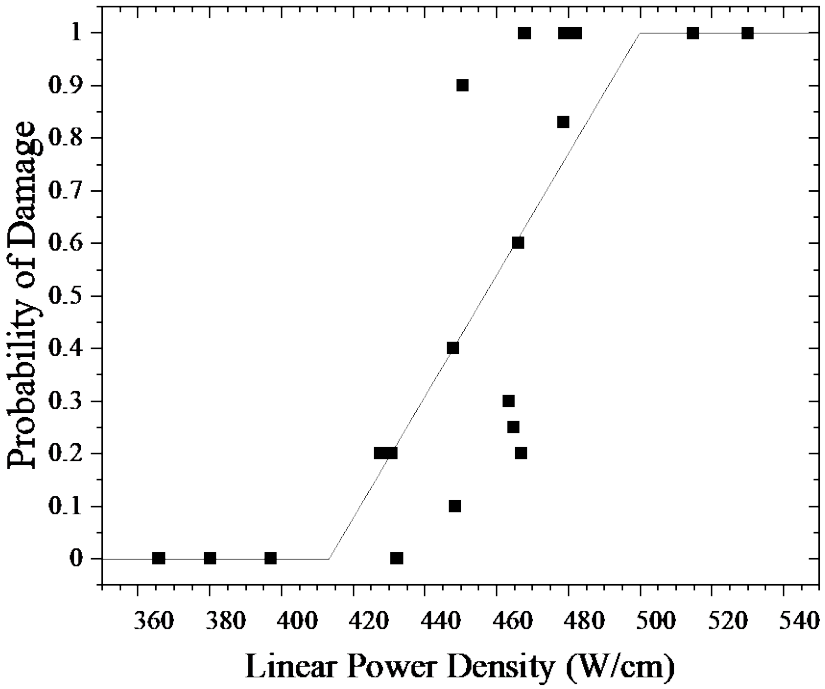

Fig. 31 Plot of the probability of damage as a function of the LPD for the Amorphous Materials Inc AMTIR-4 window for a 738-μm effective diameter beam with a 5-s radiation time. The straight line is the linear fit of the probability, while the blocks are the probability of damage for specific LPDs.

Figure 32 shows magnified images of two different damage spots on sample 4 using reflected light dark-field illumination with 5× and 10× magnification.

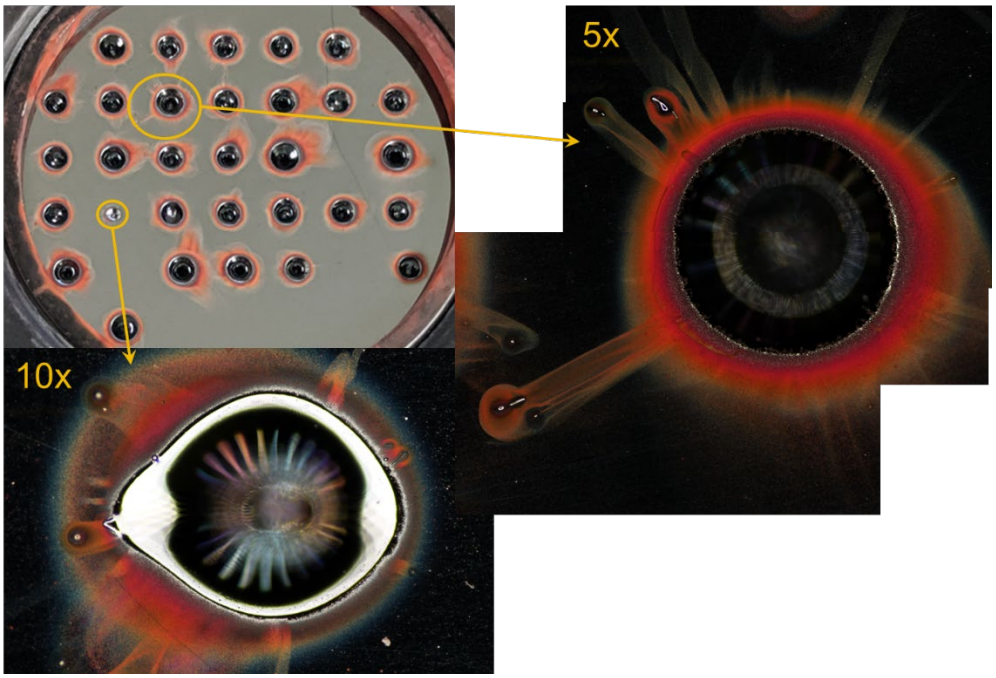

Fig. 32 Top left: AMTIR-4 sample 4. Remaining: Image of damage spots taken with a Nomarski microscope using reflected light dark-field illumination with 5× (top right) and 10× (bottom left) magnifications.

4.8 Amorphous Materials Inc AMTIR-5 (AsSe)

The CW damage results for a 5-s irradiance time on Amorphous Materials Inc AMTIR-5 are presented in Table 13. Two 1-inch-diameter, 2-mm-thick samples were tested for a range of powers with 10 runs for each individual power with an effective diameter of 587 µm (Gaussian diameter of 830 µm). The optical flats were manufactured by Amorphous Materials Inc, shipped on 22 February 2019, and are melt no. 18-C5-207. All measurements were conducted on 9 August 2019.

Table 13 Damage results for different power densities and the probability of damage for AMTIR-5

Sample no.	Linear power density (W/cm)	No damage	Damage	Probability of damage
1	306.6	0	10	1.00
1	291.1	6	4	0.40
1	281.3	7	3	0.30
1	272.3	8	2	0.20
1	253.7	9	1	0.10
2	239.7	10	0	0.00
2	298.7	7	3	0.30
2	300.5	6	4	0.40
2	304.7	4	6	0.60

The powers ranged from a power below the highest power for which no damage occurred on any of the runs (14 W) to a power above the lowest power for which damage occurred on all 10 runs (18 W). All damage reported was large and visible to the naked eye, as can be seen in the images for each of the two samples; see Fig. 33. The majority of damage spots made it all the way through to the back surface of the sample.

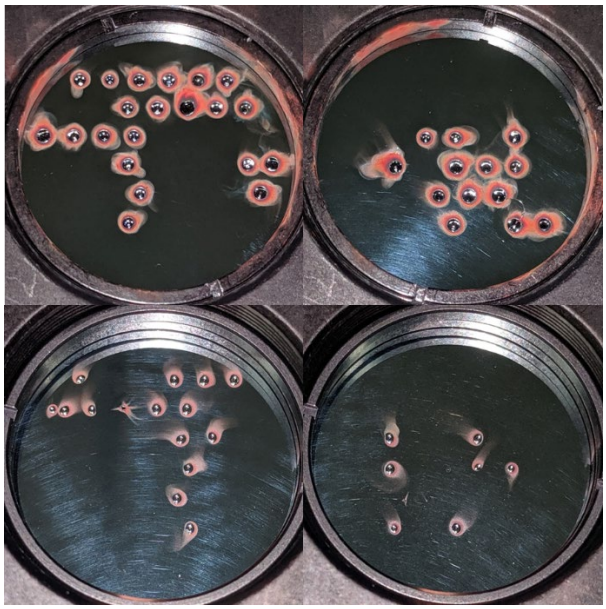

Fig. 33 Top row: Front surface of the two AMTIR-5 test samples after testing. Bottom row: Back surface of the two samples after testing.

Plotting the data (Fig. 34), we estimate the damage threshold, D_t, for an effective diameter of 587 μm and a radiation time of 5 s, to be 240 W/cm, and the damage threshold with 90% likelihood, $D_{t,90}$, to be 307 W/cm.

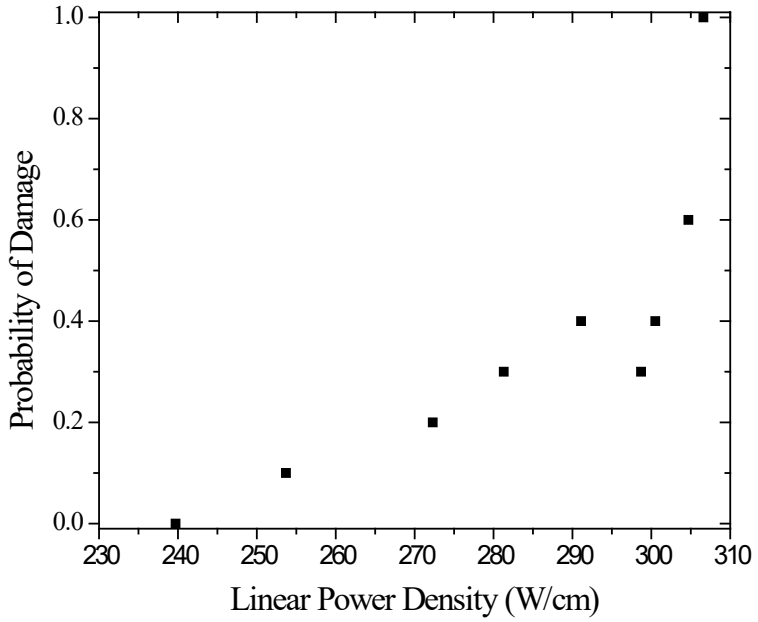

Fig. 34 Plot of the probability of damage as a function of the LPD for the Amorphous Materials Inc AMTIR-5 window for a 587-µm effective diameter beam with a 5-s radiation time

4.9 Amorphous Materials Inc AMTIR-6 (As_2S_3)

The CW damage results for a 5-s irradiance time on Amorphous Materials Inc AMTIR-6 are presented in Table 14. Ten 1-inch-diameter, 2-mm-thick samples were tested for a range of powers with 10 runs for each individual power with an effective diameter of 738 µm (Gaussian diameter of 1044 µm). The optical flats were manufactured by Amorphous Materials Inc, shipped on 22 February 2019, and are melt no. 16-A6-1. All measurements were conducted 13–17 August 2020. Data is only shown for 8 of the 10 samples. The first sample—tested at lower powers and a smaller spot size—showed no damage, while the second sample was used for initial damage testing with varying irradiance/dwell times.

Table 14 Damage results for different power densities and the probability of damage for AMTIR-6. Note that LPD is expressed in terms of kilowatts instead of watts.

Sample no.	Linear power density (kW/cm)	No damage	Damage	Probability of damage
3	2.51	4	6	0.60
3	2.51	5	5	0.50
3	2.39	4	6	0.60
4	2.33	9	1	0.10
4	2.41	9	1	0.10
4	2.49	8	2	0.20
5	2.17	9	1	0.10
5	2.07	7	3	0.30
5	1.85	10	0	0.00
6	1.94	8	2	0.20
6	1.73	9	1	0.10
6	1.50	10	0	0.00
7	1.62	9	1	0.10
7	2.87	4	6	0.60
7	3.09	3	7	0.70
8	3.56	1	9	0.90
8	3.79	0	10	1.00
8	1.27	10	0	0.00
9	3.98	1	9	0.90
9	4.28	0	10	1.00
9	4.14	1	9	0.90
10	4.48	0	10	1.00

The powers ranged from a power below the highest power for which no damage occurred on any of the runs (94 W) to a power above the lowest power for which damage occurred on all 10 runs (331 W). All damage reported was large and visible to the naked eye, as can be seen in the images for nine of the samples; see Figs. 35 and 36. As with the IRG-27, because of the large debris field that accompanied the damage, more space is left between damage spots and rows than with previous samples. Additionally, as can be seen from the Fig. 35 and 36 images, the debris was sometimes very expansive; therefore, the samples were cleaned off between some runs before proceeding to the next row or spot.

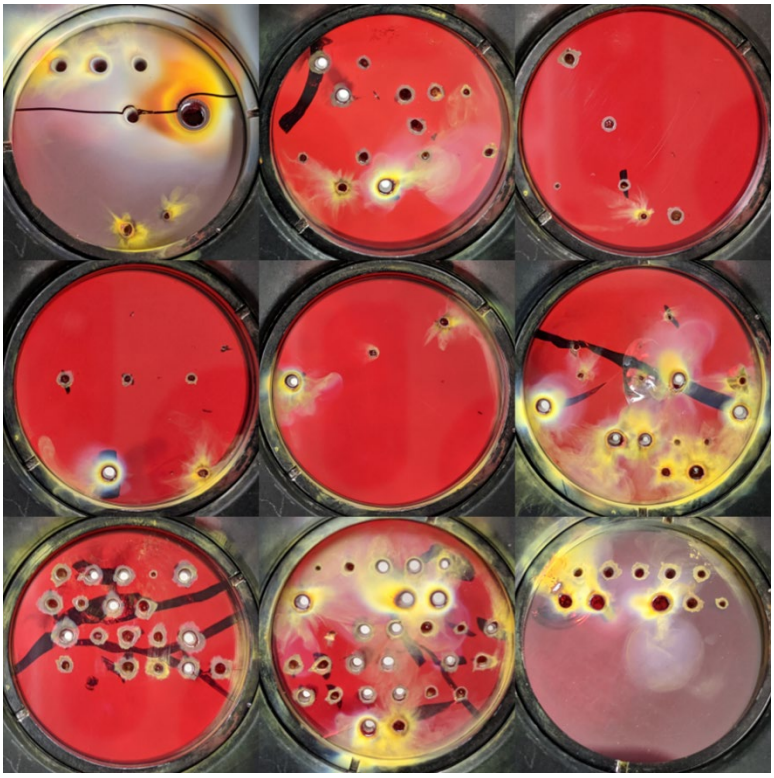

Fig. 35 Front surface of nine of the AMTIR-6 test samples after testing

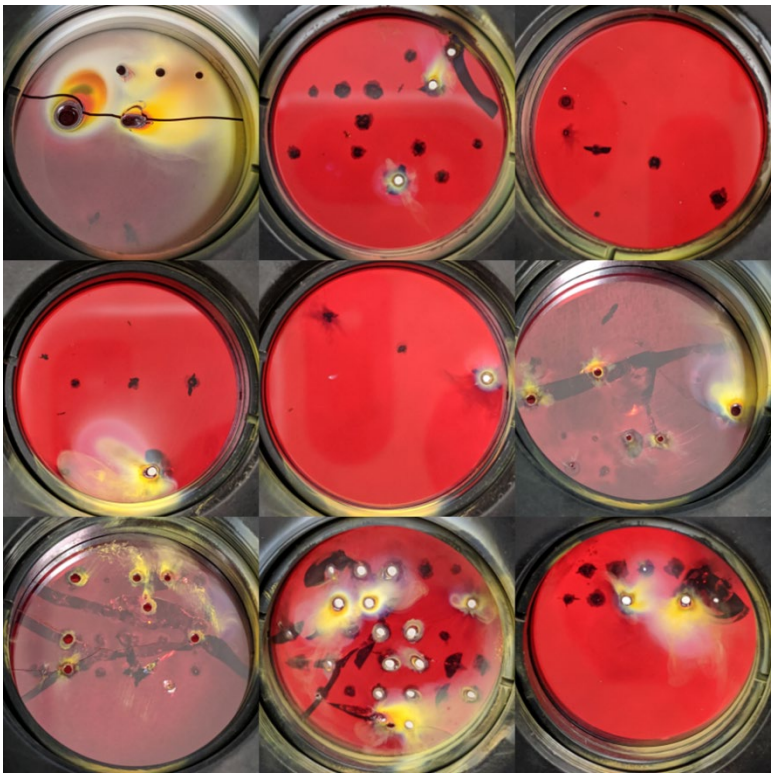

Fig. 36 Back surface of nine of the AMTIR-6 test samples after testing

Figure 37 shows two damage spots from sample 3 imaged with a Nomarski microscope with 5× magnification. Looking through some of the AMTIR-6 samples (the only samples we can see internally using visible light, other than the IRG-27) with the microscope, we did notice (not shown) some minor internal damage in areas that were not obviously damaged on the surface. This may indicate that either some of the damage starts internally or that there were impurities within the sample that burned up without causing further damage to the sample.

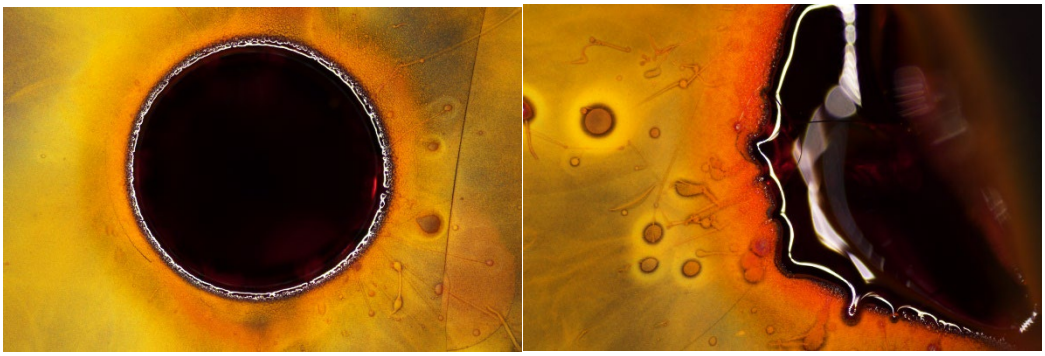

Fig. 37 Two damage spots from the AMTIR-6 sample 3 imaged with a Nomarski microscope using reflected light dark-field illumination with 5× magnification

Plotting the data (Fig. 38) and fitting it to a linear curve, we estimate the damage threshold, D_t, for an effective diameter of 738 μm and a radiation time of 5 s, to be 1.5 kW/cm, and the damage threshold with 90% likelihood, $D_{t,90}$, to be 4.1 kW/cm.

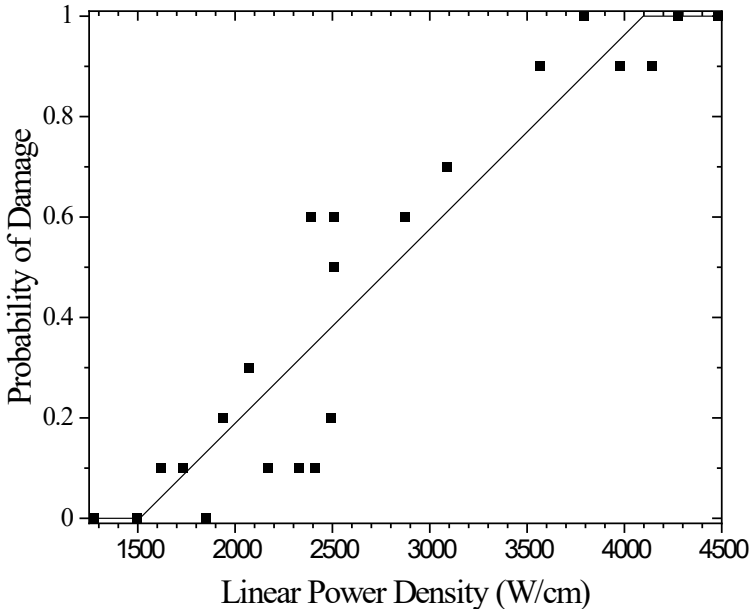

Fig. 38 Plot of the probability of damage as a function of the LPD for the Amorphous Materials Inc AMTIR-6 window for a 738-µm effective diameter beam with a 5-s radiation time. The straight line is the linear fit of the probability, while the blocks are the probability of damage for specific LPDs.

4.10 Amorphous Materials Inc AMTIR-7 (AsSe)

The CW damage results for a 5-s irradiance time on Amorphous Materials Inc AMTIR-7 are presented in Table 15. Four 1-inch-diameter, 2-mm-thick samples were tested for a range of powers with 10 runs for each individual power with two different beam spot sizes: an effective diameter of 587 µm (Gaussian diameter of 830 µm) and an effective diameter of 738 µm (Gaussian diameter of 1044 µm). For the initial testing, with the first two samples, our 1-kW laser was used, while for the latter two samples, our 1.5-kW laser, which had finer computer control of the power, was used. The optical flats were manufactured by Amorphous Materials Inc, shipped on 22 February 2019, and are melt no. 14-C7-3. All measurements were conducted between 13 August 2019 and 6 August 2020.

Table 15 Damage results for different power densities and the probability of damage for AMTIR-7

Sample no.	Linear power density (W/cm)	No damage	Damage	Probability of damage
1	306.0	0	10	1.00
1	272.8	1	9	0.90
1	255.3	2	8	0.80
1	238.8	7	3	0.30
1	222.9	10	0	0.00
2	249.6	10	0	0.00
3	180.2	10	0	0.00
3	191.7	10	0	0.00
3	207.5	10	0	0.00
3	240.5	3	0	0.00
4	239.2	5	5	0.50
4	254.7	0	10	1.00
4	269.8	0	10	1.00

The powers ranged from a power below the highest power for which no damage occurred on any of the runs (13.1 W) to a power above the lowest power for which damage occurred on all 10 runs (20.3 W). All damage reported was large and visible to the naked eye, as can be seen in the images for three of the samples tested; see Fig. 39.

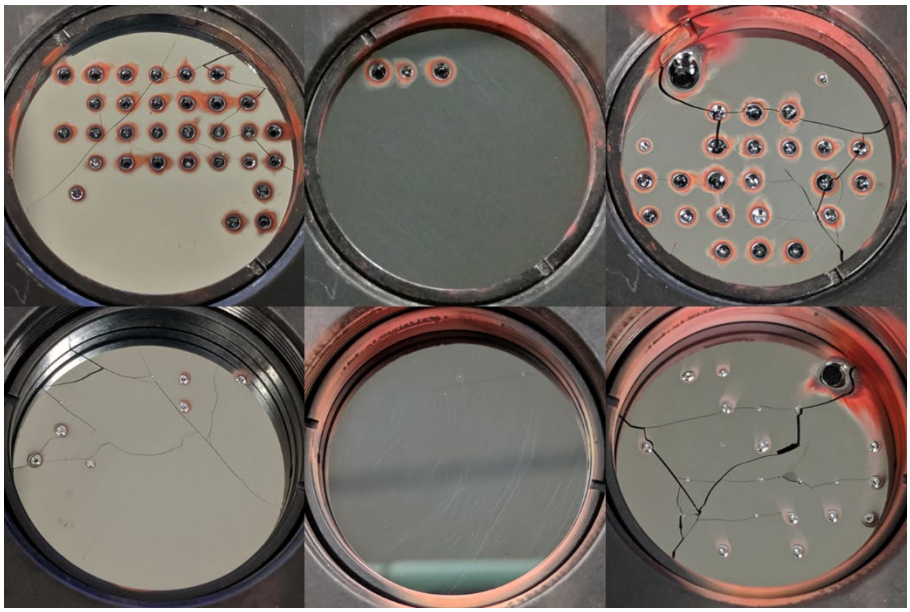

Fig. 39 Top row: Front surface of the AMTIR-7 samples 1, 3, and 4 after testing (sample 2 exhibited no damage on the 10 test sites). Bottom row: Back surface of the three samples after testing.

Plotting the data (Fig. 40) and fitting it to a linear curve, we estimate the damage threshold, D_t, for an effective diameter between 587 and 738 μm and a radiation time of 5 s, to be 217 W/cm, and the damage threshold with 90% likelihood, $D_{t,90}$, to be 281 W/cm.

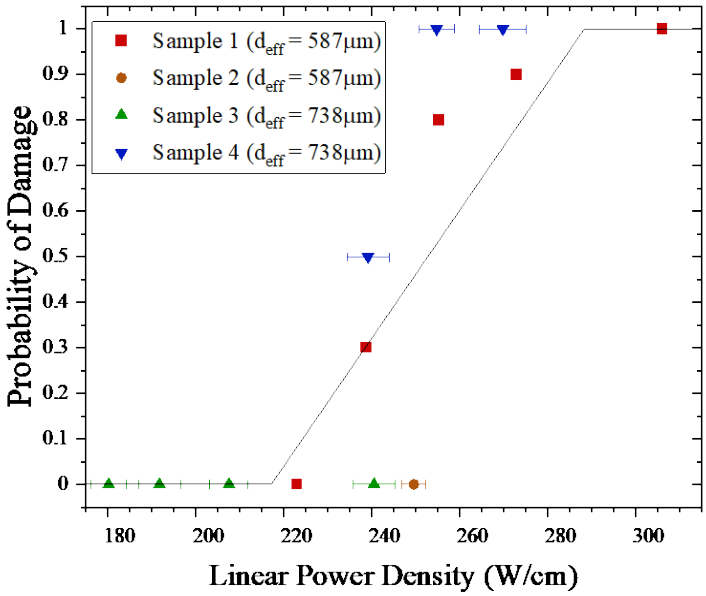

Fig. 40 Plot of the probability of damage as a function of the LPD for the Amorphous Materials Inc AMTIR-7 window for an effective diameter between 587 and 738 μm with a 5-s radiation time. The straight line is the linear fit of the probability, while the blocks are the probability of damage for specific LPDs.

Figure 41 shows the magnified images of two different damage spots on sample 4 using reflected light dark-field illumination with 5× and 10× magnification.

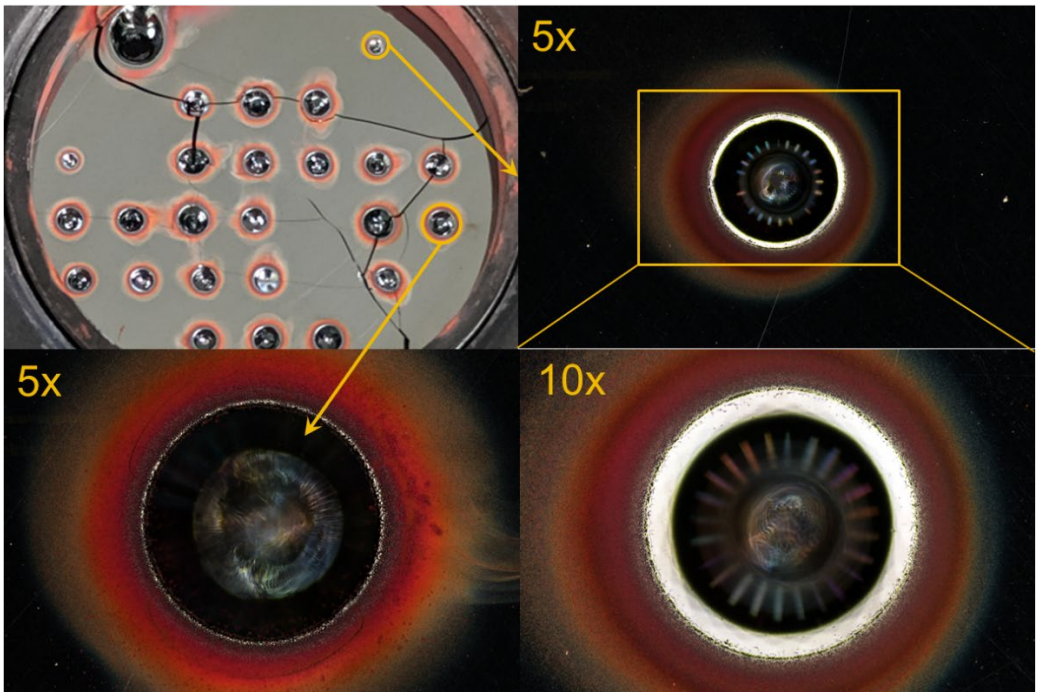

Fig. 41 Top left: AMTIR-7 sample 1. Remaining: Image of damage spots taken with a Nomarski microscope using reflected light dark-field illumination with 5× and 10× magnifications.

5. Simulation Analysis of Experimental Results

5.1 Analysis of Experimental Results

By plotting all damage curves on the same plot (Fig. 42), we can draw some broad conclusions. Overall, the Amorphous Materials Inc ChGs tested have a higher damage threshold than the SCHOTT ChGs tested. The thickness of the samples should not have a significant impact on the damage threshold; however, it cannot be discounted that the SCHOTT ChGs tested had a thickness of 3 mm compared to the Amorphous Materials Inc ChGs, which had a thickness of 2 mm. Future studies should directly compare two optics from different manufacturers with the same material composition and the same thickness. Among all the samples tested, only the AMTIR-2 and IRG-26 (As_2Se_3) and AMTIR-6 and IRG-27 (As_2S_3) share the exact same composition.

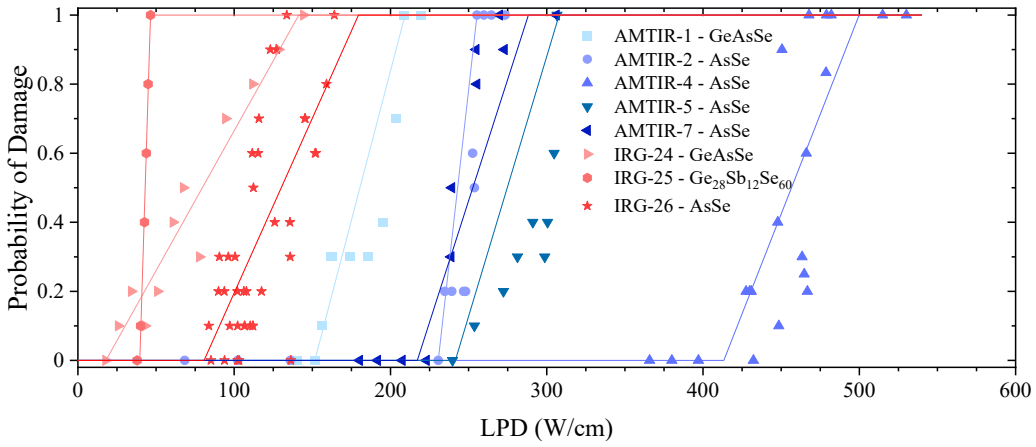

Fig. 42 Plot of the probability of damage as a function of the LPD for all samples tested, except for IRG-27 and AMTIR-6, which had a significantly higher damage threshold

Of all the samples, the IRG-25 (GeSbSe) had the steepest damage-threshold curve with a range from possible damage to 90% chance of damage at 7 W/cm compared to the rest, which have a range between 25 and 138 W/cm. Among the SCHOTT and Amorphous samples, the AsSe compositions tend to have a higher damage threshold than their Ge-containing ternary (GeAsSe and GeSbSe) counterparts, which are considered more "suitable" for IR sensor systems. Further studies would need to be done to determine if this is due to the Ge itself or the specific combination of materials.

Among the AsSe Amorphous Materials Inc ChGs—while we do not have the exact composition—we do know that the amount of arsenic decreases from AMTIR-2 to AMTIR-5 and then to AMTIR-7 with AMTIR-4 having the least arsenic (and most selenium). No clear trend is seen here, although the AMTIR-4 with the least amount of arsenic does have the highest damage threshold.

Looking at the damage on the back surface of the Amorphous Materials Inc samples, we see that the GeAsSe AMTIR-1 has the smallest damage spot sizes, while, of the As-Se composition ChGs, the AMTIR-4 with the least arsenic has the largest damage spot size. Since AMTIR-4 has the largest damage threshold, the larger spot sizes may be due to the higher powers needed to start damage and then burning through the optic more quickly. More damage is seen on the back side of the Amorphous Materials Inc ChGs than the SCHOTT ChGs; however, the SCHOTT ChGs are 1 mm thicker. See Fig. 43.

Fig. 43 Back face of the Amorphous Materials Inc ChGs. Top row, left to right: AMTIR-1, AMTIR, 2, and AMTIR-5. Bottom row, left to right: AMTIR-7, AMTIR-4, and AMTIR-6. The As-Se composition ChGs are listed in order of decreasing arsenic.

Of all the samples tested, the arsenic sulfide (As_2S_3) samples had the highest damage threshold by far (Fig. 44), being in the kilowatt range compared to the rest ranging from 5 to 240 W.

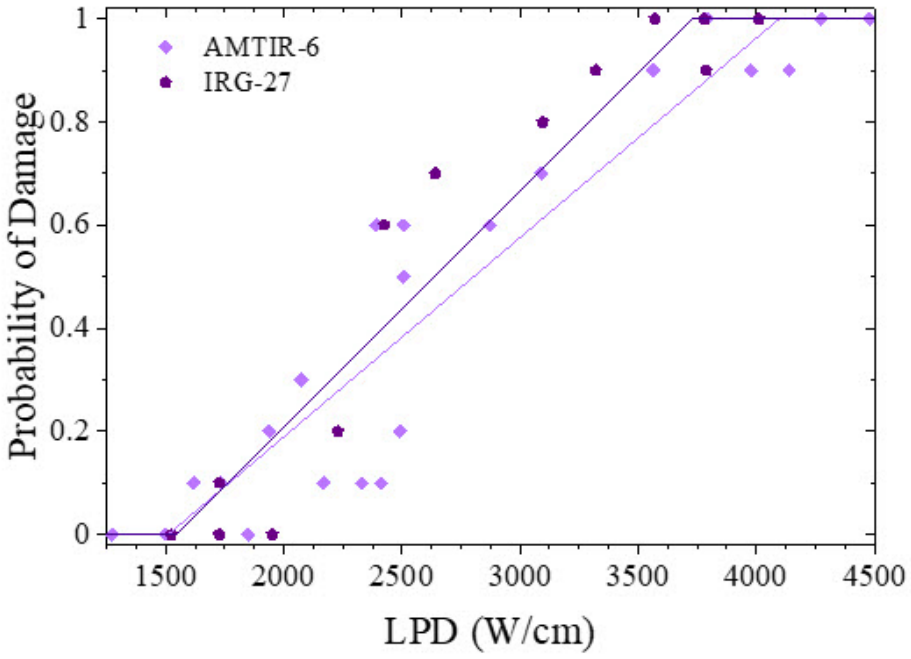

Fig. 44 Plot of the probability of damage as a function of the LPD for the AsS compositions, AMTIR-6 and IRG-27

5.2 Simulation Analysis of Experimental Results

A summary of our calculations, simulations (for 5 s and 10 min), and experimental results (both for the damage threshold and the LPD at which there is a 90% chance of damage) are shown in Table 16 with all values in linear power density (W/cm).

Table 16 The calculated, simulated, and experimental damage threshold LPDs for all ChGs tested; all are in units of W/cm

SAMPLE	CALC	SIM. (5 S)	SIM. (10 MIN)	EXP. (D_T)	EXP. ($D_{T,90}$)
IRG-24	52	688	341	5.1	130
IRG-25	20.3	248	124	39.6	46
IRG-26	20	258	127	81	170
IRG-27	127	1230	557	1540	3730
AMTIR-1	391	982	478	153	208
AMTIR-2	55	581	297	230	255
AMTIR-4	74	806	375	413	491
AMTIR-5	62	741	377	240	307
AMTIR-6	165	2186	976	1500	4100
AMTIR-7	34	419	206	217	281

Overall, our experimental results fall somewhere between the calculated estimates and the simulations for t = 5 s, often being closer to the steady state simulation estimates. To better determine why our experimental results match the steady state simulations more closely than those run for an irradiance of 5 s, matching our experimental conditions, we look at simulations using the experimental LPDs.

Simulations for most of the ChGs look similar to that of AMTIR-5, shown in Fig. 45. Looking at the maximum temperature reached in the sample for an irradiance of 5 s (top) and comparing the results from the experimental damage threshold values, D_t and $D_{t,90}$ (blue and orange lines, respectively), to those expected from the simulation-determined estimate (yellow line), we see that the simulations show that the AMTIR-5 sample should not be heating up nearly enough to reach the glass-transition temperature (indicated by the green-dashed line). This indicates that either our model is off, or the chalcogenide is damaging before it reaches the glass-transition temperature.

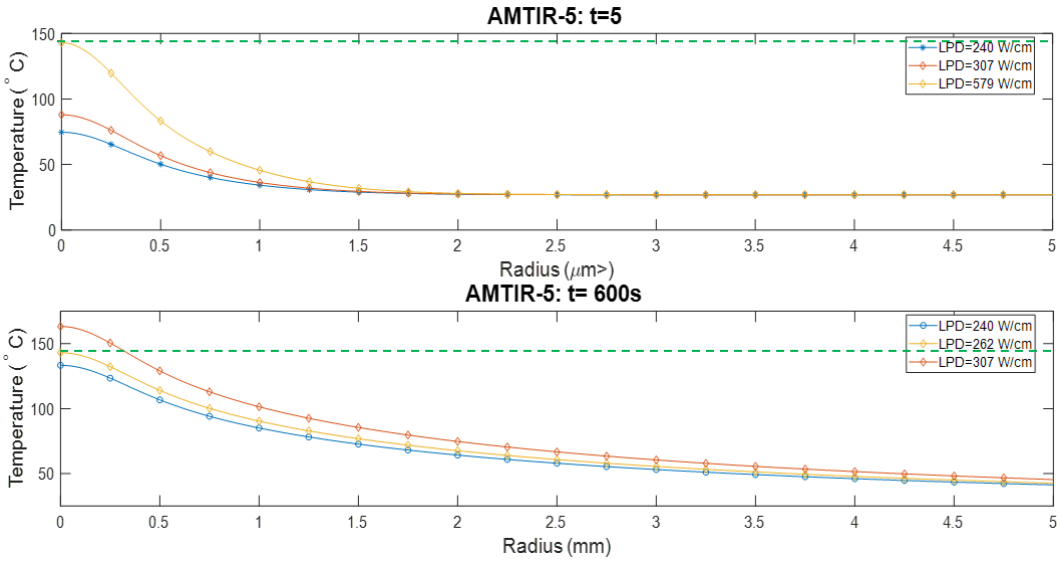

Fig. 45 Plot of temperature from the center of the AMTIR-5 sample to the edge for an irradiance time of 5 s (top) and 10 min (bottom) approaching steady state. Plot lines are for the experimental damage threshold values D_t (blue) and $D_{t,90}$ (orange) and the simulation-determined threshold values (yellow).

Looking at the maximum temperature reached in the sample for an irradiance time (10 min), approaching steady state (bottom plot), and comparing the results from the experimental damage threshold values, D_t and $D_{t,90}$ (blue and orange lines, respectively), to those expected from simulations (yellow line), we see that the results are very close. Here, we are inputting our experimental values obtained for a 5-s irradiance and running the simulation for 10 min and we see the model heating up to roughly the glass-transition temperature. This indicates that the sample may be heating up more quickly than the modeling accounts for and reaching steady state conditions significantly more quickly. To verify this, more experiments would need to be conducted.

It is worth pointing out that, experimentally, thermal lensing of the beam transmitted through the optic and onto the beam dump has been noticed, but not quantified. All of this indicates that the model may need to account for the material properties of the chalcogenides changing with a change in temperature.

6. Summary and Conclusions

We have determined the CW LIDT (Table 17) for 10 different commercially available chalcogenides for an irradiance time of 5 s using a wavelength of 1.07 μm, complimenting Norm Comer's (2016) work in the mid- and long-wave IR.

Table 17 The CW LIDT for an irradiance time of 5 s presented in terms of power, LPD, and irradiance. Damage thresholds were measured using a beam spot with an effective diameter of 587 µm, except those with an asterisk (*), which were measured using a beam spot with an effective diameter of 738 µm.

	D_T			$D_{T,90}$		
SAMPLE	**Power (W)**	**LPD (W/cm)**	**I (kW/cm^2)**	**Power (W)**	**LPD (W/cm)**	**I (kW/cm^2)**
IRG-24	0.3	5.1	0.1	7.6	130	2.8
IRG-25	2.3	39.6	0.9	2.7	46	1.0
IRG-26	4.8	81.0	1.8	10.0	170	3.7
IRG-27*	114	1540	26.6	275.3	3730	64.4
AMTIR-1	8.9	153	3.3	12.25	208	4.5
AMTIR-2	13.5	230	2.0	15.0	255	5.5
AMTIR-4*	30.5	413	7.13	30.5	491	8.5
AMTIR-5	14.0	240	5.0	18.0	307	6.7
AMTIR-6*	110.7	1500	25.9	302.58	4100	70.7
AMTIR-7*	16.0	217	3.8	20.8	281	4.9

The As-S compositions, IRG-27 and AMTIR-6, have the highest damage threshold of the chalcogenides tested by far, in the kilowatt range. The ternary compositions, which all have Ge (IRG-24, IRG-25, and AMTIR-1), have the lowest damage thresholds.

As some chalcogenides are exposed to humidity and/or light, thermal properties of the material may change, resulting in a corresponding change to the CW damage threshold.

Additionally, we have constructed a model, which between a 5-s and 10-min (steady state) irradiance time, gives us a value close to that obtained through experiment, though further refinement is necessary.

Ideally, further studies would include an investigation into the CW LIDT dependence on both the spot size of the laser beam on the sample and the thickness of the sample. For those chalcogenides whose thermal properties change with exposure to humidity and light, it would be particularly beneficial to determine a point of saturation.

7. References

Comer ND. Results of laser damage measurements on infrared optical materials. Army Research Laboratory (US); 2016 Sep. Report No.: ARL-TN-0787.

Eggleton B, Luther-Davies B, Richardson K. Chalcogenide photonics. Nature Photon. 2011;5:141–148. doi: 10.1038/nphoton.2011.309.

Fecht HJ. Thermodynamic properties of amorphous solids—glass formation and glass transition—(overview), materials transactions. JIM. 1995;36(Issue 7):777–793. doi: 10.2320/matertrans1989.36.777.

Frantz JA, Myers JD, Bekele RY, Spillmann CM, Kolacz J, Gotjen H, Nguyen VQ, McClain CC, Sanghera JS. Arsenic selenide thin film degradation and its mitigation. Opt Mater Express. 2018;8:3659–3665.

ISO 11254:2011. Lasers and laser-related equipment—determination of laser-induced damage threshold of optical surface. International Organization for Standardization; 15 July 2011a. p. 1–4.

ISO 21254:2011. Lasers and laser-related equipment—test methods for laser-induced damage threshold. International Organization for Standardization; 2011b. p. 1–4.

McElhenny JE, Bambha NK. Continuous wave laser induced damage threshold of AMTIR-1, 2, 5 and 7 chalcogenide windows at 1.07 microns. Proc. SPIE 11514, Laser-induced Damage in Optical Materials 2020; 2020 Nov 9. p. 115141F. doi: 10.1117/12.2572934.

McElhenny JE, Bambha NK. Continuous wave laser-induced damage threshold of Schott IRG-24, IRG-25, and IRG-26 at 1.07 microns. Proc. SPIE 11173, Laser-induced Damage in Optical Materials 2019; 2019a Nov 20. p. 111731I. doi: 10.1117/12.2532062.

McElhenny JE, Bambha NK. CW laser-induced damage threshold of Schott IRG-25 & IRG-26 chalcogenide optics at 1.07 microns. 2019 MSS Parallel Conference (Passive, BSD, and M&D); 2019b Feb 25–28.

McElhenny JE, Bambha NK. Results of continuous-wave laser damage measurements on Schott IRG-25 chalcogenide optic at 1.07 μm. Army Research Laboratory (US); 2018 Sep. Report No.: ARL-TR-8502.

Nguyen VQ, Sanghera JS, Kung FH, Aggarwal ID, Lloyd IK. Effect of temperature on the absorption loss of chalcogenide glass fibers. Applied Optics. 1999 May 20;38(15):3206–3213.

Ristau D. Laser induced damage in optical materials. CRC Press; 2014. ISBN-13: 978-1439872161.

SCHOTT Spec Sheet. Infrared chalcogenide glass IRG25. SCHOTT North America; 2018 [accessed 2022 Sep]. https://www.schott.com/en-nz/products/ir-materials-p1000261/downloads.

Slinker K, Pitz J, Sihn S, Vernon JP. Determining and scaling continuous-wave, laser-induced damage thresholds of thin reflectors. Opt Express. 2019;27:4748–4757.

Wood RM. (2003). Laser-induced damage of optical materials. Institute of Physics. doi: org/10.1201/9781420034059.

Zhou T, Zhu Z, Liu X, Liang Z, Wang X. A review of the precision glass molding of chalcogenide glass (ChG) for infrared optics. Micromachines. 2018;9:337. doi: 10.3390/mi9070337.

Appendix. Raw Data

Table A-1 Damage results for different power densities and the probability of damage for the SCHOTT IRG-24 samples

Sample no.	Linear power density (W/cm)	Power (W)	Irradiance (kW/cm^2)	No damage	Damage	Probability of damage
1	67.5	4.0	1.5	5	5	0.50
1	60.9	3.6	1.3	6	4	0.40
1	50.9	3.0	1.1	8	2	0.20
1	43.0	2.5	0.9	9	1	0.10
1	34.1	2.0	0.7	. . .	. . .	. . .
2	34.2	2.0	0.7	8	2	0.20
2	25.8	1.5	0.6	9	1	0.10
2	17.8	1.0	0.4	10	0	0.00
2	77.8	4.6	1.7	7	3	0.30
2	94.5	5.5	2.0	3	7	0.70
3	111.8	6.6	2.4	2	8	0.80
3	128.4	7.5	2.8	1	9	0.90
3	144.4	8.5	3.1	0	10	1.00

Table A-2 Damage results for different power densities and the probability of damage for the SCHOTT IRG-25 samples

Linear power density (W/cm)	Power (W)	Irradiance (kW/cm^2)	No damage	Damage	Probability of damage
37.9	2.20	0.82	10	0	0.0
40.2	2.33	0.87	9	1	0.1
42.6	2.49	0.92	6	4	0.4
43.8	2.56	0.95	4	6	0.6
44.9	2.63	0.97	2	8	0.8
46.5	2.72	1.01	0	10	1.0

Table A-3 Damage results for different power densities and the probability of damage for the SCHOTT IRG-26 samples

Sample no.	Linear power density (W/cm)	Power (W)	Irradiance (kW/cm^2)	No damage	Damage	Probability of damage
1	106.6	6.3	2.31	9	1	0.10
1	102.2	6.0	2.22	9	1	0.10
1	97.2	5.7	2.11	9	1	0.10
1	90.5	5.3	1.96	7	3	0.30
1	85.2	5.0	1.85	10	0	0.00
2	89.9	5.3	1.95	8	2	0.20
2	96.3	5.7	2.09	7	3	0.30
3	102.0	6.0	2.21	8	2	0.20
3	112.0	6.6	2.43	9	1	0.10
3	123.1	7.2	2.67	1	9	0.90
4	115.8	6.8	2.51	3	7	0.70
4	115.3	6.8	2.50	4	6	0.60
4	112.4	6.6	2.44	5	5	0.50
5	106.7	6.3	2.32	9	1	0.10
5	107.8	6.3	2.34	8	2	0.20
5	102.1	6.0	2.22	10	0	0.00
6	127.2	7.5	2.76	1	9	0.90
6	133.6	7.8	2.90	0	10	1.00
7	83.8	4.9	1.82	9	1	0.10
7	93.7	5.5	2.03	8	2	0.20
7	100.6	5.9	2.18	7	3	0.30
7	111.6	6.6	2.42	4	6	0.60
8	106.2	6.2	2.30	8	2	0.20
8	111.9	6.6	2.43	9	1	0.10
8	117.5	6.9	2.55	8	2	0.20
8	126.0	7.4	2.73	6	4	0.40
9	136.3	8.0	2.96	10	0	0.00
9	145.5	8.5	3.16	3	7	0.70
9	151.8	8.9	3.29	4	6	0.60
9	159.0	9.3	3.45	2	8	0.80
10	164.1	9.6	3.56	0	10	1.00
10	152.2	8.9	3.30	4	6	0.60
10	145.2	8.5	3.15	3	7	0.70
11	135.7	8.0	2.94	6	4	0.40
11	135.9	8.0	2.95	7	3	0.30
11	93.9	5.5	2.04	10	0	0.00
11	103.2	6.1	2.24	10	0	0.00
11	110.2	6.5	2.39	9	1	0.10

Table A-4 Damage results for different power densities and the probability of damage for the SCHOTT IRG-27 samples

Sample no.	Linear power density (kW/cm)	Power (W)	Irradiance (kW/cm^2)	No damage	Damage	Probability of damage
1	2.23	164.5	38.5	8	2	0.20
1	1.95	144.0	33.7	10	0	0.00
1	1.73	127.5	29.8	9	1	0.10
2	1.73	127.5	29.8	10	0	0.00
2	2.64	195.0	45.6	3	7	0.70
3	3.10	228.5	53.4	2	8	0.80
3	3.57	263.5	61.6	0	10	1.00
4	3.32	245.0	57.3	1	9	0.90
4	3.79	279.5	65.3	1	9	0.90
5	1.52	112.5	26.3	10	0	0.00
5	2.43	179.0	41.8	4	6	0.60
6	3.78	279.0	65.2	0	10	1.00
7	4.01	296.0	69.2	0	10	1.00

Table A-5 Damage results for different power densities and the probability of damage for the Amorphous Materials Inc AMTIR-1 samples

Sample no.	Linear power density (W/cm)	Power (W)	Irradiance (kW/cm^2)	No damage	Damage	Probability of damage
1	162.4	9.53	3.5	7	3	0.30
1	140.0	8.22	3.0	10	0	0.00
1	151.6	8.9	3.3	10	0	0.00
1	174.3	10.23	3.8	7	3	0.30
1	185.3	10.875	4.0	7	3	0.30
2	195.4	11.47	4.2	6	4	0.40
2	219.8	12.9	4.8	0	10	1.00
2	208.6	12.245	4.5	0	10	1.00
2	203.7	11.955	4.4	3	7	0.70
2	161.9	9.505	3.5	7	3	0.30
3	156.4	9.18	3.4	9	1	0.10

Table A-6 Damage results for different power densities and the probability of damage for the Amorphous Materials Inc AMTIR-2 samples

Sample no.	Linear power density (W/cm)	Power (W)	Irradiance (kW/cm^2)	No damage	Damage	Probability of damage
1	68.4	4.02	1.48	10	0	0.00
1	102.3	6.01	2.22	10	0	0.00
1	135.9	7.98	2.95	10	0	0.00
1	239.3	14.05	5.19	8	2	0.20
1	273.4	16.05	5.93	0	10	1.00
2	253.7	14.89	5.50	5	5	0.50
2	246.8	14.49	5.35	8	2	0.20
2	264.6	15.53	5.74	0	10	1.00
2	259.8	15.25	5.64	0	10	1.00
3	255.4	14.99	5.54	0	10	1.00
3	252.6	14.83	5.48	4	6	0.60
3	248.1	14.57	5.38	8	2	0.20
3	230.6	13.54	5.00	10	0	0.00
3	234.8	13.79	5.09	8	2	0.20

Table A-7 Damage results for different power densities and the probability of damage for the Amorphous Materials Inc AMTIR-4 samples

Sample no.	Linear power density (W/cm)	Power (W)	Irradiance (kW/cm^2)	No damage	Damage	Probability of damage
2	365.9	27.0	6.3	10	0	0.00
2	380.1	28.05	6.6	10	0	0.00
2	397.0	29.3	6.8	10	0	0.00
2	427.5	31.55	7.4	8	2	0.20
3	429.9	31.725	7.4	8	2	0.20
3	448.5	33.1	7.7	9	1	0.10
3	466.8	34.45	8.1	8	2	0.20
3	478.7	35.325	8.3	1	5	0.83
4	479.0	35.35	8.3	0	10	1.00
4	467.8	34.525	8.1	0	10	1.00
4	450.5	33.25	7.8	1	9	0.90
4	430.9	31.8	7.4	8	2	0.20
5	432.2	31.9	7.5	10	0	0.00
5	447.8	33.05	7.7	6	4	0.40
5	466.1	34.4	8.0	4	6	0.60
5	464.8	34.3	8.0	6	2	0.25
6	463.4	34.2	8.0	7	3	0.30
6	482.0	35.575	8.3	0	10	1.00
6	514.9	38.0	8.9	0	10	1.00
6	530.1	39.125	9.1	0	10	1.00

Table A-8 Damage results for different power densities and the probability of damage for the Amorphous Materials Inc AMTIR-5 samples

Sample no.	Linear power density (W/cm)	Power (W)	Irradiance (kW/cm^2)	No damage	Damage	Probability of damage
1	306.6	18.0	6.7	0	10	1.00
1	291.1	17.085	6.3	6	4	0.40
1	281.3	16.515	6.1	7	3	0.30
1	272.3	15.985	5.9	8	2	0.20
1	253.7	14.895	5.5	9	1	0.10
2	239.7	14.07	5.2	10	0	0.00
2	298.7	17.535	6.5	7	3	0.30
2	300.5	17.64	6.5	6	4	0.40
2	304.7	17.885	6.6	4	6	0.60

Table A-9 Damage results for different power densities and the probability of damage for the Amorphous Materials Inc AMTIR-6 samples

Sample no.	Linear power density (kW/cm)	Power (W)	Irradiance (kW/cm^2)	No damage	Damage	Probability of damage
3	2.51	185.0	43.2	4	6	0.60
3	2.51	185.0	43.2	5	5	0.50
3	2.39	176.5	41.3	4	6	0.60
4	2.33	172.0	40.2	9	1	0.10
4	2.41	178.0	41.6	9	1	0.10
4	2.49	184.0	43.0	8	2	0.20
5	2.17	160.0	37.4	9	1	0.10
5	2.07	153.0	35.8	7	3	0.30
5	1.85	136.5	31.9	10	0	0.00
6	1.94	143.0	33.4	8	2	0.20
6	1.73	128.0	29.9	9	1	0.10
6	1.50	110.5	25.8	10	0	0.00
7	1.62	119.5	27.9	9	1	0.10
7	2.87	212.0	49.6	4	6	0.60
7	3.09	228.0	53.3	3	7	0.70
8	3.56	263.0	61.5	1	9	0.90
8	3.79	280.0	65.5	0	10	1.00
8	1.27	94.0	22.0	10	0	0.00
9	3.98	293.5	68.6	1	9	0.90
9	4.28	315.5	73.8	0	10	1.00
9	4.14	305.5	71.4	1	9	0.90
10	4.48	330.5	77.3	0	10	1.00

Table A-10 Damage results for different power densities and the probability of damage for the Amorphous Materials Inc AMTIR-7 samples

Sample no.	Linear power density (W/cm)	Power (W)	Irradiance (kW/cm^2)	No damage	Damage	Probability of damage
1	306.0	17.97	6.6	0	10	1.00
1	272.8	16.02	5.9	1	9	0.90
1	255.3	14.98	5.5	2	8	0.80
1	238.8	13.98	5.2	7	3	0.30
1	222.9	13.09	4.8	10	0	0.00
2	249.6	14.8	5.4	10	0	0.00
3	180.2	13.6	3.1	10	0	0.00
3	191.7	14.5	3.3	10	0	0.00
3	207.5	15.63	3.6	10	0	0.00
3	240.5	18.1	4.1	3	0	0.00
4	239.2	18.0	4.1	5	5	0.50
4	254.7	19.1	4.4	0	10	1.00
4	269.8	20.3	4.7	0	10	1.00

List of Symbols, Abbreviations, and Acronyms

2-/3-D	two-/three-dimensional
ARL	Army Research Laboratory
As	arsenic
As_2Se_3	arsenic triselenide
C5ISR	Command, Control, Computers, Communications, Cyber, Intelligence, Surveillance, and Reconnaissance
ChGs	chalcogenide glass
CW	continuous wave
DEVCOM	US Army Combat Capabilities Development Command
DIC	differential interference contrast
Ga	gallium
Ge	germanium
HiPo CoW	High Power Continuous Wave
IR	infrared
ISO	International Organization for Standardization
KILTE	Kilowatt Interlocked Light-Tight Enclosure
LIDT	laser-induced damage threshold
LPD	linear power density
NVESD	Night Vision and Electronic Sensors Directorate
P	phosphorus
S	sulfur
Se	selenium
Si	silicon
Te	tellurium
TFP	thin film polarizer

1 (PDF) DEFENSE TECHNICAL INFORMATION CTR DTIC OCA

1 (PDF) DEVCOM ARL FCDD RLD DCI TECH LIB

12 (PDF) DEVCOM ARL FCDD RLS CL
J MCELHENNY
N BAMBHA
N BARBIERI
T ENSLEY
N GUPTA
R HOFFMAN
J MCELHENNY
A MOTT
R O'DONNELL
Z QUINE
T ROHRABAUGH
W SHENSKY

4 (PDF) US ARMY CERDEC RDER NVESD
M SNYDER
C DUNN
A DOTSON
C KNICK

2 (PDF) US ARMY GVSC
J D'ARCHANGEL
T WHITTAKER

2 (PDF) DAC
B ODOM
P BROWN

3 (PDF) DEVCOM AC
D MARIANUCCI
J HITSCHERICH
S ZUBER

5 (PDF) US AIR FORCE RESEARCH LAB
J VERNON
K SLINKER
J PITZ
R ULIBARRI
M SHEYKA

3 (PDF) SMDTC
C LAMAR
N FLORES
G ROMANCZUK

4 (PDF) US USN NAVAL SURFACEWARFARE CENTER
C LLOYD
C WILSON
D SPOOR
T MORGAN

2 (PDF) US NRL
D GIBSON
L BUSSE

2 (PDF) JH/APL
J MIRAGLIOTTA
D SHREKENHAMER

1 (PDF) DNL CONSULTING
D LOOMIS

2 (PDF) RADIANCE TECH
D DUFFIN
D LYMAN

4 (PDF) SCHOTT
C LAKEMAN
J MARRO
K ROZENBERG
N CARLIE

1 (PDF) AMORPHOUS MATERIALS
T LORETZ

2 (PDF) UCF CREOLE
K RICHARDSON
M RICHARDSON

1 (PDF) PENN STATE ARL
J THOMAS

1 (PDF) TRITON SYSTEMS
M MURACHVER

1 (PDF) LIGHTPATH
S NOVAK

1 (PDF) UNCC
I STAVENGER

1 (PDF) IR FLEX
F CHENARD